V.I. Il`icev Pacific Oceanological Institute

Far East Branch, Academy of Sciences of Russia

Vladivostok, Russian Federation

Transmission Loss Studies on the North East Sakhalin Shelf

2001 and 2002

Sakhalin, Russian Federation

M.V. Kruglof

A.N. Rutenko

Prepared for

Exxon Neftegas Limited
&
Sakhalin Energy Investment Company

Yuzhno-Sakhalinsk, Sakhalin,

Russian Federation

30 November 2003

Table of Contents

LIST OF FIGURES II
LIST OF TABLES IV
EXECUTIVE SUMMARY V
1 INTRODUCTION 1
1.1 Acoustic recording and processing equipment 2
1.2 Low Frequency (LF) electromagnetic resonance transducer 3
1.3 Terminology and algorithms used in the report 6
1.4 Units 7
2 THEORETICAL AND EXPERIMENTAL STUDIES OF ACOUSTIC PROPAGATION 8
2.1 Theoretical analysis of sound propagation in shallow water 8
3 EXPERIMENTAL ANALYSIS OF SOUND PROPAGATION FROM THE MOLIKPAQ AREA TO PILTUN BAY 29
4 EXPERIMENTAL ANALYSIS OF SOUND PROPAGATION SEAWARD OF THE CHAYVO AREA 39
5 CONCLUSIONS 52
6 FUTURE PLANS 54
7 ACKNOWLEDGEMENTS 55
8 AUTHORS 55
9 BIBLIOGRAPHY 56
APPENDIX A - TL FOR PROPAGATION PARALLEL AND PERPENDICULAR TO THE COAST 58
APPENDIX B - DESCRIPTION OF DATA USED FOR THE TL STUDIES 62

LIST OF FIGURES

Figure 1.1 Low frequency resonance transducer and calibrated monitor hydrophone being deployed from the *Irbis.*

Figure 1.2 Spectra *G(f)* of 24 Hz (and harmonics) LF data recorded synchronously on sonobuoys at locations b.1 and b.3 [2002] and the calibrated reference hydrophone (G_0) 2 m from the transducer.

Figure 2.1 Model of a waveguide with parameters similar to those on the NE Sakhalin shelf and the results of normal mode TL modeling for frequencies of 30 Hz, 100 Hz and 300 Hz.

Figure 2.2 Sonograms *G(f,t)* of anthropogenic noise synchronously recorded at locations a.1, a.2 and a.5 (analog sonobuoys) on September 13-14, 2002.

Figure 2.3 Spectra *G(f)* of anthropogenic acoustic noise synchronously at locations a.1, a.2 and a.5 (analog sonobuoys) on 14 September 2002.

Figure 2.4 Sonograms *G(f,t)* and spectra *G(f)* of anthropogenic acoustic noise synchronously at locations a.1, a.2 and a.5 (analog sonobuoys). This noise was monitored as the *Okha* approached the Molikpaq platform on 14 September 2002.

Figure 2.5 Sonograms *G(f,t)* and spectra *G(f)* of anthropogenic noise recorded at locations b.1 and b.2 (digital sonobuoys) on 23 September 2002.

Figure 2.6 Spectra *G(f)* of acoustic noise synchronously recorded at locations a.1 and a.2 (digital sonobuoys) on 17 September 2002.

Figure 2.7 Spectra *G(f)* of ambient noise recorded at locations b.1 and b.2 (digital sonobuoys) on 21 September 2002.

Figure 2.8 Map showing the layout of the Transmission Loss experiments.

Figure 2.9 Time domain, frequency domain and frequency-time (sonogram) plots of impulses from the *Nordic Explorer* recorded on the *Grif* and by sonobuoy T.6.

Figure 2.10 Amplitude spectra synchronously recorded by sonobuoys at locations T.4 and T.5 (1.88 km apart). Figure 3.1 - Map of the study area showing

the locations of sonobuoys (a.1 .. a.5), and the source locations (i.1 .. i.5) where the *Irbis* was located.

Figure 3.2 Bathymetric profile of the study area showing the locations of sonobuoys a.1, a.2, a.4 and a.5.

Figure 3.3 Spectra *G(f)* of HF data recorded synchronously from a reference hydrophone plus analog sonobuoys at locations a.4 and a.5.

Figure 3.4 Spectra *G(f)* of LF data recorded synchronously on sonobuoys at locations a.1 (digital), a.2 and a.5 (analog).

Figure 3.5 Regression results from the Molikpaq-Piltun Transmission Loss experiments.

Figure 4.1 Map of the study area showing the locations of sonobuoys (b.1, b.2 and b.3) and the source locations for the *Irbis* as well as an approximate location for the offshore gray whale feeding area.

Figure 4.2 Bathymetric profile of the study area showing the locations of sonobuoys (b.1, b.2 and b.3) and the *Irbis*.

Figure 4.3 Spectra *G(f)* of low frequency (24 Hz and harmonics) data recorded synchronously on a reference hydrophone 2 m from the transducer and sonobuoys at locations b.1 (digital), and b.3 (analog).

Figure 4.4 Regression results from the Chayvo Transmission Loss experiments.

Figure 4.5 Spectra *G(f)* of ambient and anthropogenic noise recorded at locations b.1, b.2 and b.3 (analog and digital sonobuoys) on 23 September 2002.

Figure 4.6 Plots of RTL_{max} calculated with Equation (12) using noise generated by the *Trias* and recorded on sonobuoys b.1, b.2 (digital), and b.3 (analog).

Figure 4.7 Plots of $RTL_{average}$ calculated with Equation (10) using noise generated by the *Trias* and recorded on sonobuoys b.1, b.2 (digital), and b.3 (analog).

Figure 4.8 Plots of $RTL_{average}$ calculated with Equation (10) using noise generated by the *Trias* and recorded on sonobuoy b.2 (digital).

Figure 4.9 Chayvo acoustic model showing the model parameters.

Figure 4.10 Experimental and Model RTL data from the Chayvo acoustic experiment.

Figure 4.11 **Plot of RTL vs Range for the *Trias* experiment of 23 September, the data were plotted on Figure 4.7.**

LIST OF TABLES

Table 3.1 **TL estimates from the 15 September 2002 experiment.**

Table 3.2 **TL estimates from the 16 September 2002 experiment.**

Table 3.3 **TL estimates from the LF experiment.**

Table 3.4 **Regression results from Molikpaq-Piltun data.**

Table 4.1 **TL estimates from the 22 September 2002 experiment.**

Table 4.2 **TL estimates from the 21 and 22 September 2002 experiments (resonant tones and harmonics).**

Executive Summary

Environmental Impact Assessments (EIA) conducted prior to the development of the oil and gas resources off the NE Sakhalin coast determined that the key marine environmental issue is protection of western gray whales (*Eschrichtius robustus*)[1]. Since 1997, Exxon Neftegas Limited (ENL) and Sakhalin Energy Investment Company (SEIC) have been conducting acoustic and biological studies to determine the possibility that the development could impact the sensitive Korean Okhotsk Gray whale population.

Aerial surveys from 1997 to 2001 indicated that gray whales spend most of the ice-free season feeding off the NE Sakhalin coast. They are predominantly located shoreward of the 20 m water depth contour, in an area from the mouth of Piltun Bay and northwards along the NE Sakhalin coast. In 2001, a second feeding area south of the Arktun-Dagi license in 30-45 m of water was observed in aerial and shipboard surveys.

The Justification of Investment (JOI) SEER panel has requested that the cumulative impact of the planned development on this population be investigated with specific focus on the impact of low frequency sound. To this end acoustic data was evaluated to determine the frequency dependent transmission loss between the Vityaz production complex and mouth of Piltun Bay. Due to the improved performance of the digital sonobuoys (improved response and dynamic range), and the more detailed profiles recorded in 2002, this data was predominantly used to estimate transmission loss. Impulsive data recorded in 2001 was used to independently confirm estimates of the absorption coefficient. From this data, equations for the frequency dependent transmission loss have been defined and the range spreading and attenuation constants determined by regression.

Acoustic measurements were also made between the Chayvo barge quay and the offshore gray whale feeding area. As operational restrictions did not allow a calibrated source inshore of the shallowest sonobuoy, no absolute transmission loss measurements could be made. However, transmission loss estimates from a source in deeper water and measurements of noise from moving ships allowed a preliminary estimate of transmission loss to be made.

---

[1] The Korean Okhotsk (western) gray whale population is listed as endangered in the Russian Red Book and critically endangered by the International Union for the Conservation of Nature (IUCN).

1 Introduction

The acoustic programs conducted on the NE shelf of Sakhalin Island in 2001 and 2002 had three main objectives. The first was to evaluate and monitor the acoustic transmission from the Odoptu seismic survey (2001), the second to study both the temporal and spatial variations in the amplitude and frequency characteristics of anthropogenic acoustic noise near the mouth of Piltun Bay[2] (2001, 2002) and near Chayvo Bay (2002). The third was to study the frequency dependent transmission loss of noise generated in the vicinity of the Molikpaq platform and near Chayvo Bay. The first objective was discussed in a report [Borisov et al., 2002][1], the second in two separate reports [Borisov et al., 2003][2,3].

The third objective, to study the frequency dependent Transmission Loss (TL) of noise generated in the vicinity of the Molikpaq platform and near Chayvo Bay is the subject of this report. Broadband and tonal TL measurements were made along a transect between the Molikpaq platform and the mouth of Piltun Bay and from Chayvo Bay to the offshore gray whale feeding area discovered in 2001. Broadband noises generated by vessels (especially the *Irbis* and *Trias*), a low frequency (LF) (24-33 Hz) resonance transducer and a high frequency (HF) (800-10,000 Hz) transducer, both with known acoustic characteristics, were used in these studies.

The results of TL studies previously discussed in Borisov et.al. [2002] have also been included in Appendix A of this report for completeness, since this report discusses all other TL studies conducted by POI on the NE Sakhalin shelf in the last two years.

These TL studies use acoustic measurements recorded on the continental shelf of the Okhotsk Sea, between Molikpaq and the mouth of Piltun Bay between 17-24 September 2001 and 12-19 September 2002. Data recorded between 21-23 September 2002 from the mouth of Chayvo Bay seaward was also used. Most of the data used in this report is from the 2002 acoustic program as the sonobuoys had a greater bandwidth and dynamic range. However, where appropriate, results from the 2002 acoustic program have been compared with those from the 2001 acoustic program.

---

[2] The mouth of Piltun Bay is one of the summer feeding grounds for the Korean-Okhotsk (western) gray whale.

1.1 Acoustic recording and processing equipment

Individually deployed autonomous sonobuoys were used to measure acoustic signals in the frequency band from 10 Hz to 5 kHz (2001) and 1 Hz to 10 kHz (2002). Practical experience has shown that at shallow deployment depths (10-30 m), wave action can create significant noise at the hydrophone. Movement of the sonobuoy due to surface waves is mechanically conducted down the wire to the hydrophone, where this mechanical movement is recorded as acoustic noise. To reduce this noise, the hydrophone is deployed at a distance from the anchor, thus reducing the mechanical coupling between the surface buoy and the hydrophone. The sub-sea component of the system consists of a hydrophone, pre-amplifier and frequency dependent gain correction. The hydrophone is deployed inside a pyramid shaped wire frame and attached by rubber bands to the corners of the frame, isolating it to the best extent possible from the sea floor.

In 2001, only analog sonobuoys were used; these transmitted the analog signals to a shore station (Piltun lighthouse) via radio. Analog data received at the shore station was converted to digital data by an analog to digital converter (ADC) and accumulated in a digital format on the hard drive of a laptop computer. A detailed description of the characteristics and calibration of the 2001 acoustic recording equipment is provided elsewhere [Borisov et al., 2002, 2003][1,2].

In 2002, the acoustic measurements were made using analog and digital sonobuoys developed at POI FEB RAS[3]. Analog sonobuoys were used to record frequencies from 10 Hz to 10 kHz and digital sonobuoys from 1 Hz to 2.5 kHz. When used together an analog and digital sonobuoy pair can record acoustic data from 1 Hz to 10 kHz. The radio signals from the analog and digital buoys were received at one of two recording stations; one was at Piltun lighthouse and the other on the *Irbis* (which was stationed near the Molikpaq platform). The range of the digital radio channel was over 4 km when received by the antenna on the *Irbis* and over 7 km when received at Piltun lighthouse. The range of the analog radio channel depended on the type of radio receiver used. Broadband (10-10,000 Hz) signals could be transmitted up to 12 km; narrowband (10-5000 Hz) signals could be transmitted up to 20 km if received by the station at Piltun lighthouse. A detailed

[3] POI FEB RAS - The Pacific Oceanological Institute, Far East Branch of the Russian Academy of Sciences.

description of the characteristics and calibration of the 2002 acoustic recording equipment is provided elsewhere [Borisov et al., 2003][3].

To compute TL from acoustic measurements made by different sonobuoys, the data has to be calibrated to an absolute pressure standard. The hydrophones were manufactured with nominal sensitivities and the gains were set in the field. Field cross-calibrations conducted in 2001 & 2002 confirmed the absolute calibration of the data. Further details of the types of sonobuoys used, their location, deployment depth and recording settings can be found in Appendix B and Borisov et al., 2002, 2003 [1,2,3].

Sonobuoys were deployed from a zodiac or the support vessel *Irbis*. Signals were received on the *Irbis* or at Piltun lighthouse.

1.2 Low Frequency (LF) electromagnetic resonance transducer

A Low Frequency resonance transducer was used for the TL measurements. The LF transducer has a cylindrical container filled with gas[4], and a pair of identical closely spaced radiating pistons oscillating in opposite directions creating a volume displacement[5]. An electromagnetic controller controls the motion of the pistons; the ends of the pistons are connected together by cylindrical springs and to the edge of the cylindrical container with rubber gaskets. The transducer is powered by a bridge thyristor inverter connected to the transducer by the 4-line 34 m long cable. Hydrostatic compensation is achieved using an air pump. In order to achieve electric resonance, a battery of electric capacitors and solenoids located on board the *Irbis* are connected sequentially with the solenoid of the transducer.

Figure 1.1 shows the LF resonance transducer and calibrated reference hydrophone (G_0) being deployed over the side of the Irbis. Figure 1.2 displays the spectral levels of the acoustic field generated by the transducer at different locations for a resonance frequency of 24 Hz and its harmonics: #2 at 48 Hz and #12 at 288 Hz.

---

[4] Dimensions are: Diameter 58 cm, Height 15 cm; Weight 48 kg in air, ~6 kg in water.

[5] During calibration tests in the Sea of Japan the amplitude of the piston motion at the resonance frequency was 3.3 mm. The amplitude of the volumetric oscillation was therefore 0.0012 cubic meters. The tests using calibrated accelerometers, and conducted at a depth of 2 m, indicated that when the maximum number of springs (30) are used, the resonance frequency of the transducer is 20.2 Hz with marginal frequencies of 15.2 and 30.6 Hz (-3 dB).

The LF resonance transducers were deployed at a depth of 8 m from the anchored *Irbis* (water depth 20 m). The 28 Hz acoustic signal has an intensity of 166 dB re 1 $\mu Pa^2/Hz$ at 2 m from the transducer; the signal was recorded by all the active sonobuoys[6].

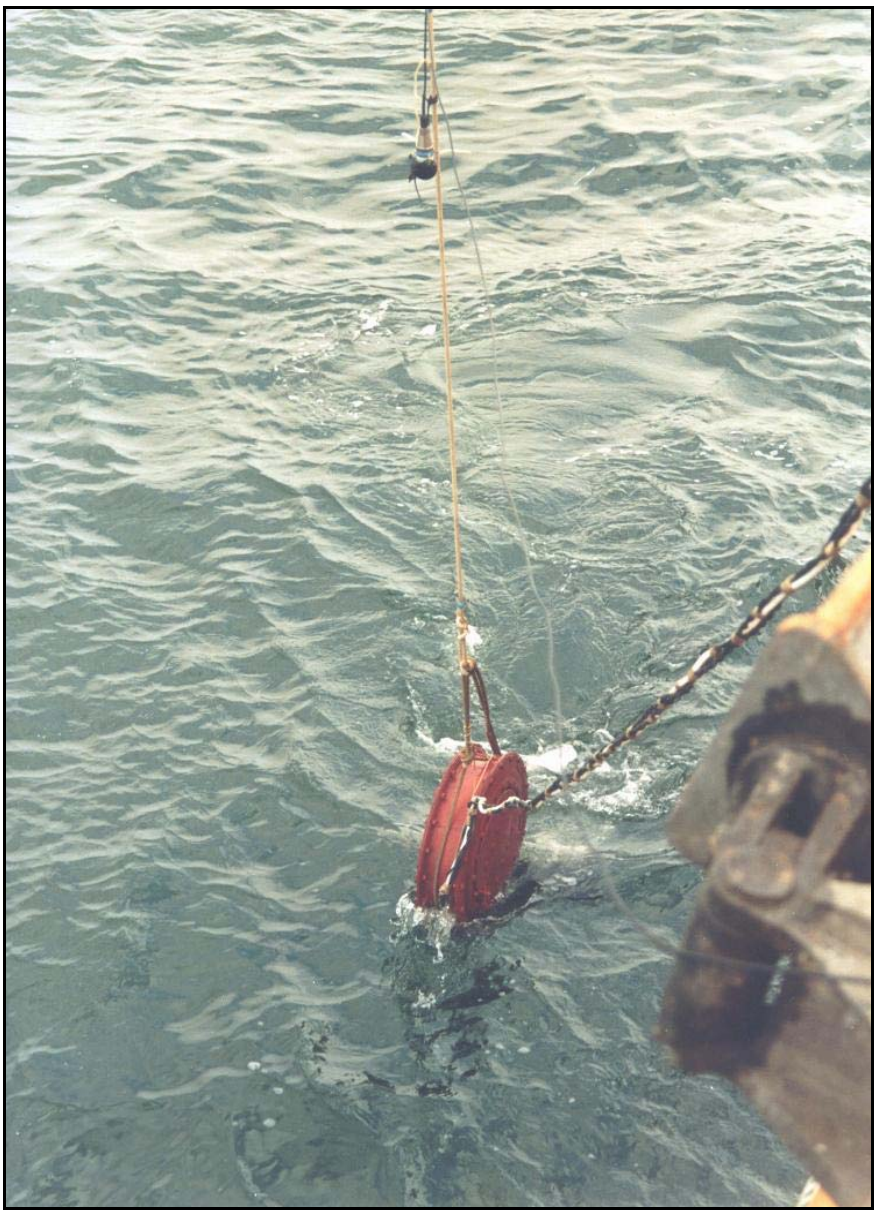

Figure 1.1 - Low frequency resonance transducer and calibrated monitor hydrophone being deployed from the *Irbis.*

[6] While the transducers were operating the acoustic signal levels were measured using a calibrated hydrophone located 1 - 2 m away from the transducer.

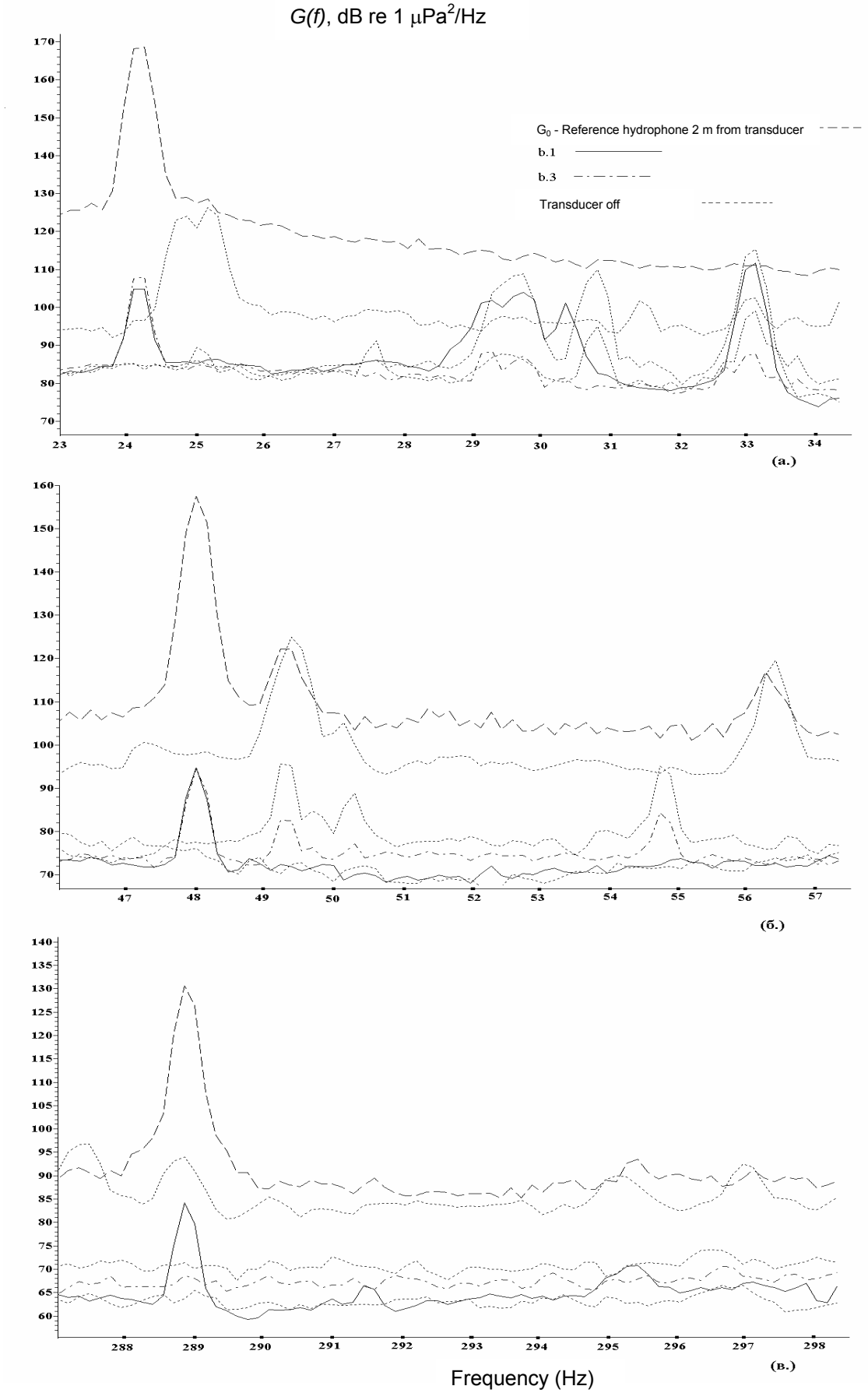

Figure 1.2 - Spectra *G(f)* of 24 Hz (and harmonics) LF data recorded synchronously on sonobuoys at locations b.1 and b.3 [2002] and the calibrated reference hydrophone (G_0) 2 m from the transducer.

1.3 Terminology and algorithms used in the report

Ambient and anthropogenic noise recorded by the sonobuoys was written to disc in microPascals (μPa)[7]. Acoustic spectra in decibels will be used to describe the variation in acoustic power as a function of frequency. In this report, sound pressure energy density spectra ($\mu Pa^2/Hz$)[8] or power density spectra ($\mu Pa^2/(s\ Hz)$)[9] will be used when spectral data are plotted.

The ***Spectral level*** of noise relates to the level of acoustic power in a 1 Hz band. This term is only applied to sounds with continuous frequency spectra[10]. These spectra are often averaged over 10-300 one-second windows[11] to improve the statistical stability of the ambient noise data[12].

The sonograms are plots of frequency vs. time, the scales generally run from ~40 to ~105 dB re 1 $\mu Pa^2/Hz$.

The acoustic measurements made by sonobuoys yield a synchronous series of spatially discrete data. This data set will allow the temporal, spatial and spectral[13] characteristics of the acoustic field to be evaluated. Noise (signal) produced by a moving vessel has a continuous spectrum with discrete tonal components. Equipment operating on the Molikpaq (gas generators, compressors, pumps, etc.) is also a source of continuous tonal and broadband acoustic noise. This could include infrasonic (<20 Hz) noise.

A detailed description of the methodology used for analyzing both the amplitude and spectral data is given in Borisov et al., 2003a.

---

[7] The data was scaled (after incorporating hydrophone sensitivity and system gain) to convert the data to standard units of pressure (measured through an omni-directional hydrophone) in real time.
[8] Energy and power spectra are scaled to 1 Hz whatever the analysis length.
[9] Acoustic intensity.
[10] A continuous frequency spectrum is a spectrum with signal present at all sampled frequencies.
[11] Average of 10 or 300 1 second spectral realizations.
[12] Spectral averaging will lead to the cancellation of zero mean errors in instrument noise leading to an improvement in the ambient noise/instrument noise level at low ambient noise levels.
[13] The spectral characteristics of the acoustic field were analyzed within the frequency range of the recording system.

1.4 Units

During the course of this report, a number of different unit notations have been used. This is due to differences in standard notation between different disciplines and nationalities.

The following are equivalent units using the different standard nomenclatures:

1 mkPa = 1 μPa

1 mkV = 1 μV

It should also be remembered that:

1 atm $\cong$ 1 bar = 0.1 MPa = 10^{11} μPa

For spectral density plots:

Although the units for power spectral density are $\mu Pa^2/(s\ Hz)$, $\mu Pa^2/s/Hz$ or μPa^2, the units for power spectral density are sometimes defined as $\mu Pa^2/Hz$ or $\mu Pa/\sqrt{Hz}$.

2 Theoretical and Experimental Studies of Acoustic Propagation

This section gives a theoretical overview of acoustic propagation in the shallow waters of the NE Sakhalin shelf. This theoretical model is calibrated using both impulsive and continuous acoustic TL data recorded in the shallow waters of the NE Sakhalin shelf.

2.1 Theoretical analysis of sound propagation in shallow water

This section gives an analytical description of acoustic propagation in the research area and describes some of the characteristics of acoustic propagation in a shallow sea. The propagation of acoustic energy in shallow water depends on a number of factors including (but not limited to) source and receiver depth, water depth, water velocity and the physical parameters of the bottom and sub bottom. The differential equations that describe the variation in the acoustic field with space and time for a realistic transmission path are difficult to solve. In estimating acoustic propagation one of two theoretical approaches are commonly used: ray theory or the theory of normal modes [Richardson et al. 1995][23].

Ray theory is most useful in deeper water (deep enough for the propagation of 10 or more modes[14]) and only requires that the medium properties do not change significantly over a Fresnel zone. The sound field is calculated by tracing rays from source to receiver, the amplitude being approximated by ray density (the amplitude fidelity is not reliable). Caustics and shadow zones can cause problems with this method and the computational load could be increased by a large number of reflected rays. Solutions (some semi-empirical) to these issues have been developed.

Normal mode theory can be used to describe how sound propagates in channels (waveguides) whose velocity changes vertically not laterally, whose boundaries repeatedly reflect the sound waves and whose boundary conditions can be specified. The existence of these boundaries constrains the propagation solutions to a set of discrete modes. The problem of solving the wave equation for a sloping or irregular bottom has been overcome by a number of methods; one is to use equations that take into account mode coupling (coupled normal mode method), another uses an approximation called the parabolic equation. The implementation of this equation uses small incremental steps in range and depth to change acoustic propagation parameters without developing large errors.

[14] A mode is an eigenvalue solution of the waveguide.

However, in deep water where large numbers of modes are propagating, this method becomes computationally cumbersome.

Each mode is characterized both by a waveguide cutoff frequency below which sound will not propagate efficiently and a vertical distribution of nulls and maxima in the sound field. The number of modes that can simultaneously exist (propagating in superposition) increases with the frequency and waveguide depth. Mode theory can be extremely useful for low frequency sounds whose wavelengths approach the depth of the waveguide.

The normal mode approximation is therefore generally used to describe the acoustic field in an inhomogeneous waveguide (such as the shallow shelf zone) [Brekhovskikh, 1974]. Only a limited number of energetic modes can propagate in shallow water where the water column acts as a waveguide, the number of these modes depends on both the ratio of water layer depth to wavelength and the vertical acoustic velocity distribution. For example, for a waveguide with an infinitely hard bottom and constant sound velocity, the maximum number of energetic (normal) modes is:

$$M \approx \frac{2\mathrm{H}}{\lambda} \qquad (1)$$

Where:
M is the number of normal modes.
H is the waveguide depth.
λ is the wavelength.

Water depth in the waveguide defines the lowest frequency that can propagate to long ranges. Every normal mode has a critical frequency [f_0], the mode exists if its frequency is greater than f_0 (i.e. for a particular water depth, normal modes with lower frequencies attenuate very rapidly when propagating in a gradually shallowing water layer)[15].

$$f_0 \approx \frac{\mathrm{c}}{4H} \qquad (2)$$

Where:
f_0 is the critical frequency.
H is the waveguide depth.
c is water velocity.

[15] For example when acoustic energy propagates in a waveguide created as the water depth gradually decreases from the shelf to the shore.

Modal attenuation increases greatly where the water layer is shallowing, when the decreasing water depth reaches the critical depth the mode structure transforms into a continuous-spectrum wave[16] and is quickly absorbed by the water bottom. If the depth is changing gradually for a constant frequency, at a specific ratio of depth to wavelength, the mode is absorbed by the bottom. Higher modes start to be absorbed by the bottom at greater water depths, the last mode to be absorbed is the first mode and the modal attenuation coefficient is proportional to H^{-3} (for all modes).

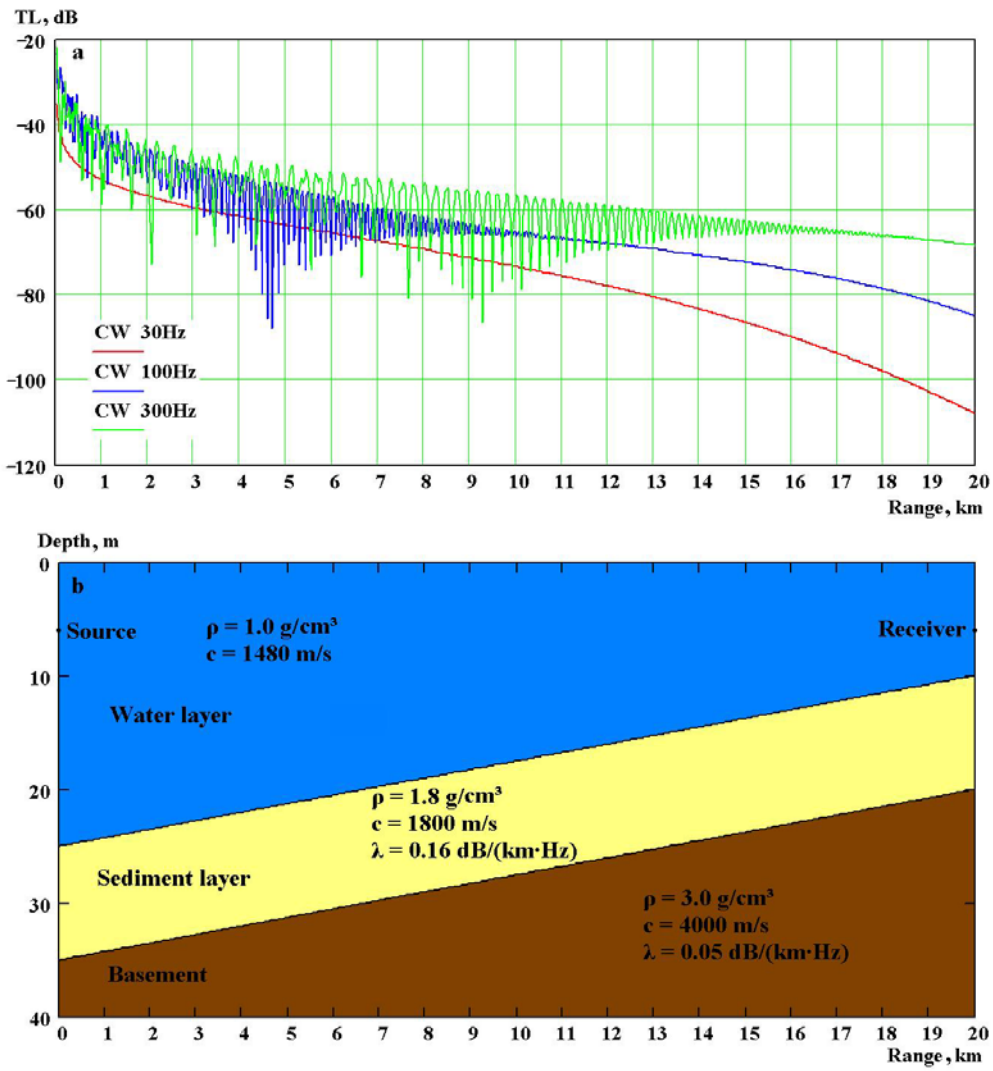

Figure 2.1 - Model of a waveguide with parameters similar to those on the NE Sakhalin shelf and the results of normal mode TL modeling for frequencies of 30 Hz, 100 Hz and 300 Hz.

[16] No mode structure with a limited number of frequencies.

Figure 2.1 shows a model of a waveguide with mechanical and acoustic parameters similar to those on the NE Sakhalin shelf. Normal mode modeling was used to compute the TL as a function of range for a source at 6 m depth, transmitting up slope to a receiver also at 6 m depth, for frequencies of 30, 100 and 300 Hz. It should be noted that the 30 Hz TL function shows only the first mode. The other two functions show intermodal interference at the shorter ranges, however the higher order modes die out as the water shallows first for 100 Hz and then for 300 Hz and only the first mode remains.

Bathymetric irregularities or variations in the water layer significantly impact sound propagation [Ashley et al., 1987]. Random fluctuations in the acoustic velocity field can cause scattering (modal transformation); this diffraction and transformation can be approximated with some models. Additionally there are losses due to the absorption of acoustic energy by the bottom [Katsnelson et al., 1997].

A literature search has shown that the following general acoustic parameters have been used to model the sound propagation in the shallow waters of the Sakhalin shelf (Figure 2.1 did not use this exact model):

Layer (I) - An unconsolidated liquid layer consisting mainly of bottom sediments such as clay and having a shear modulus close to zero. The characteristic feature of this layer is the presence of significant and random irregularities within the layer itself. The average sediment density is 1.5-2 g/cm^3 and the acoustic velocity (compressional C_l) is 1470-1900 m/s. Layer 1 is an absorbing layer, for frequencies below 1000 Hz the absorption coefficient is approximately proportional to frequency $\{\beta \propto (\beta_f . f)\}$, where the frequency dependent absorption coefficient (β_f) is between 0.01-0.3 dB/km/Hz, however at lower frequencies the absorption coefficient can be larger. Also $\beta_f \approx \beta_q f^q$ where q is a non-linear function dependent on bottom conditions.

Layer (II) - A semi-consolidated layer consisting of denser sedimentary rock (sandstone etc). The acoustic velocity $C_l \approx$ 2000-3000 m/s; shear waves with

velocities $C_t \approx 0.2C_l$ can propagate here[17]. The absorption coefficients for compressional and shear waves are variable and have values from 0.01 to 0.1 dB/km/Hz [Hampton, 1974].

Layer (III) - A consolidated layer, this bedrock (granite, basalt) layer is a semi-infinite half space extending to infinite depth ($Z=\infty$). The compressional acoustic velocity $C_l \approx$ 4000-6000 m/s; and the shear wave velocity $C_t \approx$ 1000-3000 m/s. The frequency dependent absorption coefficients are estimated as $\beta_l \approx 0.1$ dB/km/Hz and $\beta_t \approx$ 0.01-0.1 dB/km/Hz.

The layer thickness and depth can vary greatly in the model. When analyzing the attenuation of sound propagating at frequencies higher than 100 Hz for distances greater than 100 km, a homogeneous liquid half-space is generally used to define the bottom. The properties of the bottom (e.g. absorption) are therefore averaged over the whole acoustic profile. However, in the case of sound propagating over short distances, channeling in the sea-bottom should be considered [Kuperman et al. 1984].

The complexity of the model can be enhanced by the addition of both extra layers and increased detail for the acoustic and elastic properties of the bottom. Currently, there are a number of theoretical models for sound propagation in rocks, all based on Biot theory [Biot, 1956]. In Biot theory, the sediments are considered as a two component medium, a hard skeletal matrix filled with liquid. These models can be used to estimate velocities and attenuation coefficients for different types of waves and especially the frequency dependent attenuation coefficient for both compressional and shear waves. For compressional waves, this ratio is dependent on sediment properties (e.g. pressure, porosity, temperature, average particle size etc.) for modes that are affected by bottom conditions.

When a low frequency transducer is operated in shallow water it can excite shear waves in the bottom. If a shear mode can exist in either of these two media (e.g. semi-consolidated and consolidated layer), surface waves are generated travelling along the boundary

[17] The acoustic velocity of the shear waves can reach several hundred meters per second (on the Sakhalin shelf 480 m/s)

between the two media, crucially, these waves do not have a critical frequency. Ensen published an article numerically modeling a shallow waveguide containing bottom layers in which seismic waves can propagate [Ensen et al., 1985]. This model had a greater than 10 km long waveguide with a water depth of 100 m and a 5 m thick sand layer overlying bedrock. The acoustic energy for frequencies greater than 50 Hz propagated as compressional waves in the water, and at frequencies lower then 10 Hz as seismic waves in the earth. At intermediate frequencies the attenuation was greater than 40 dB (at 10 km).

In an article discussing the influence of the acoustic properties of the sediments on the seismic wavefield excited by a low frequency transducer operating on the ocean shelf; Bespalov et al. noted that estimation of acoustic field attenuation depended on the transmission frequency and model parameters selected [Bespalov et al., 1998]. Lower frequency energy passes into the semi-infinite sand half-space and is not returned back to the water layer. If a sandstone-limestone boundary replaces the semi-infinite sand half-space, there will be a sharp increase in the amplitude of the acoustic field near the water bottom[18]. At a range of 20 km, this increase can be as great as 50 dB at 1 Hz and 60 dB at 10 Hz.

Therefore, the number of normal modes excited by an industrial source is determined by the thickness of the water layer, depth of the source and acoustic properties of the bottom. Geometric dispersion within a waveguide causes each normal mode to propagate with different phase and group velocities. Geometric dispersion in a waveguide depends both on the geometry (e.g. slope of the channel) and the parameters of the waveguide. As a result, the acoustic field in the waveguide has a complex spatial interference structure with maxima and minima in both space and frequency. Also, if a broadband anthropogenic noise source is moving, the interference structure of its acoustic field will have a temporal variability. If there are a limited number of normal modes originating and propagating in the waveguide, there will be well defined maxima and minima in the spatial-frequency interference structure of the acoustic field[19].

---

[18] A hard water bottom traps more acoustic energy in the water layer.
[19] For example, transmitting the first two modes of a tonal acoustic signal with approximately equal amplitude will cause the amplitude of the acoustic field to go to zero at certain points in the waveguide.

Figures 2.2-2.4 show sonograms *G(f,t)* and spectral density plots *G(f)* of the acoustic field synchronously measured at points a.1, a.2, and a.5 (see Figure 3.1) during a period of increased operations near Molikpaq. The sonograms *G(f,t)* correspond to the time when three vessels were sailing around the *Okha* jack-up and clear maxima and minima can be seen in the frequency-spatial interference structure at frequencies under 1500 Hz (Figure 2.4). For locations a.1 and a.2, the power of the acoustic field decreased 6 dB between 200 Hz and 1200 Hz (Figure 2.3: 8:39h, 8:50h). Spectral density plots *G(f)* of acoustic signals synchronously recorded at locations a.1, a.2, and a.5 show a 'red noise' (linear) spectrum at frequencies from 1.5-5 kHz (Figure 2.3: 8:39). This 'red noise' was a result of the complex interference pattern created by the large number of normal waves propagating in the waveguide. Higher modes propagating in the shallow waveguide die out after being absorbed by the bottom. Dispersion due to bathymetric variations and spatial fluctuations in the velocity field cause the normal modes to interact with an accompanying energy transfer between modes (from lower to higher) [McDoniel, 1982; McDoniel & McCammon, 1987].

This transfer of energy to higher modes with higher losses at certain frequencies results in a sharp increase in attenuation at these frequencies [Zhou et al., 1991]. All these physical phenomena must be considered when analyzing spectra of acoustic noise synchronously recorded at different locations, especially when spectra measured near a source of broadband noise are similar to 'red' or 'white' noise spectra (e.g. spectra *G(f)* - Figure 2.5: sonobuoy b.2-D, 13:26; 13:40).

The spectral density *G(f)* plots of Figures 2.6 and 2.7 illustrate the appearance of the critical frequency for sound propagating in a waveguide with an inclined bottom. Figure 2.6 (9:51) illustrates that when low-frequency broadband noise is not being generated at locations a.1 and a.2, the spectral density plot *G(f)* does not contain a peak in the 30-100 Hz frequency band (Figures 2.6: 0:51 and 2.7: 20:31). Figure 2.6 (00:07) corresponds to a time when the vessel *Chara* was moving near location a.2, the water depth at location a.2 is approximately 19 m, so a moving vessel could effectively produce acoustic energy at frequencies up to 30 Hz (critical frequency). The spectral density plot *G(f)* for sonobuoy a.2-D (Figure 2.6: 00:07) shows a broad peak in the band between 60-110 Hz, whereas the plot for data synchronously recorded on sonobuoy a.1-D (11 m deep) (Figure 2.6: 00:07) has a minimum, the difference in the signal levels can be up to 30 dB at 90 Hz.

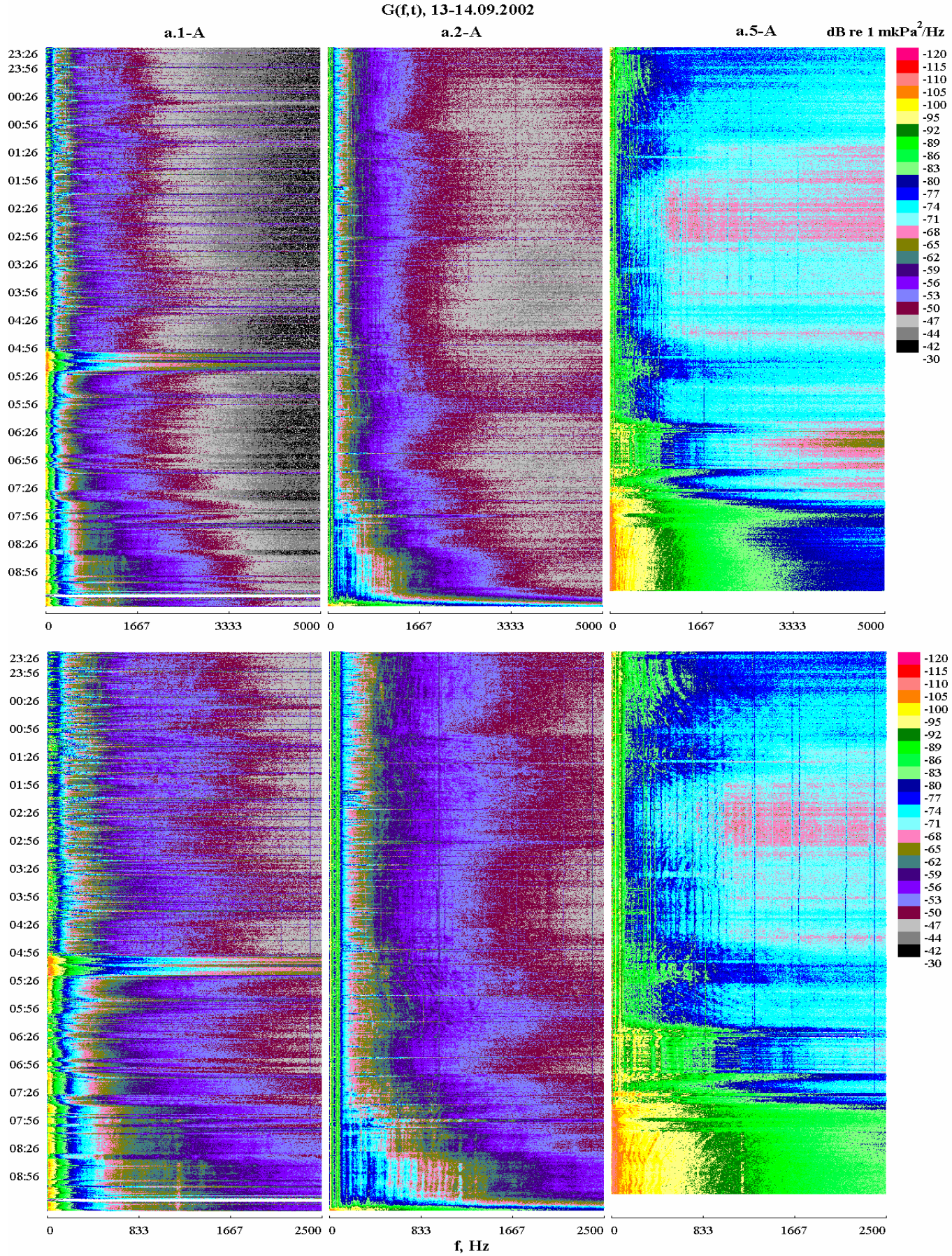

Figure 2.2 - Sonograms *G(f,t)* of anthropogenic noise synchronously recorded at locations a.1, a.2 and a.5 (analog sonobuoys) on 13-14 September 2002.

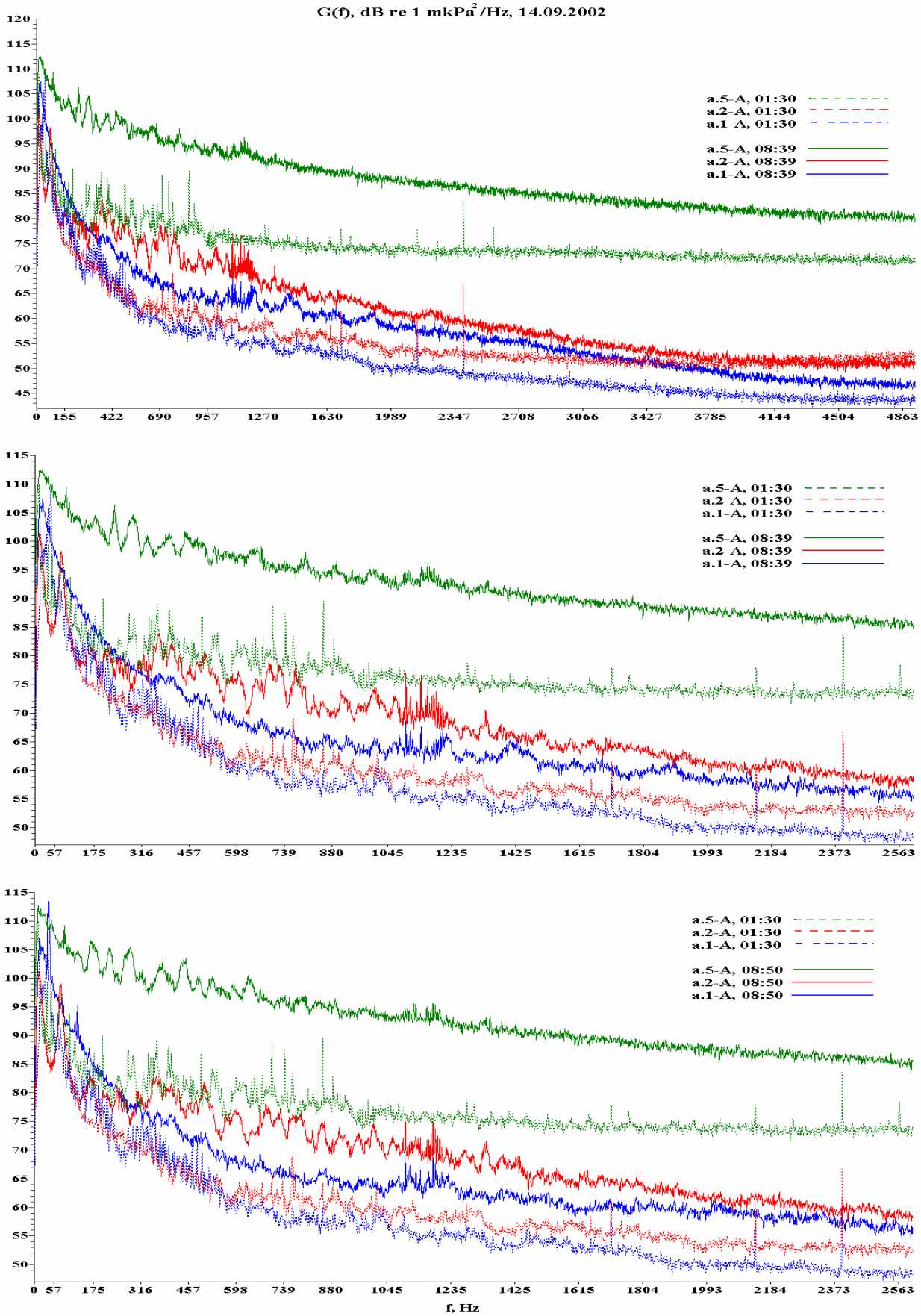

Figure 2.3 - Spectra *G(f)* of anthropogenic acoustic noise synchronously at locations a.1, a.2 and a.5 (analog sonobuoys) on 14 September 2002.

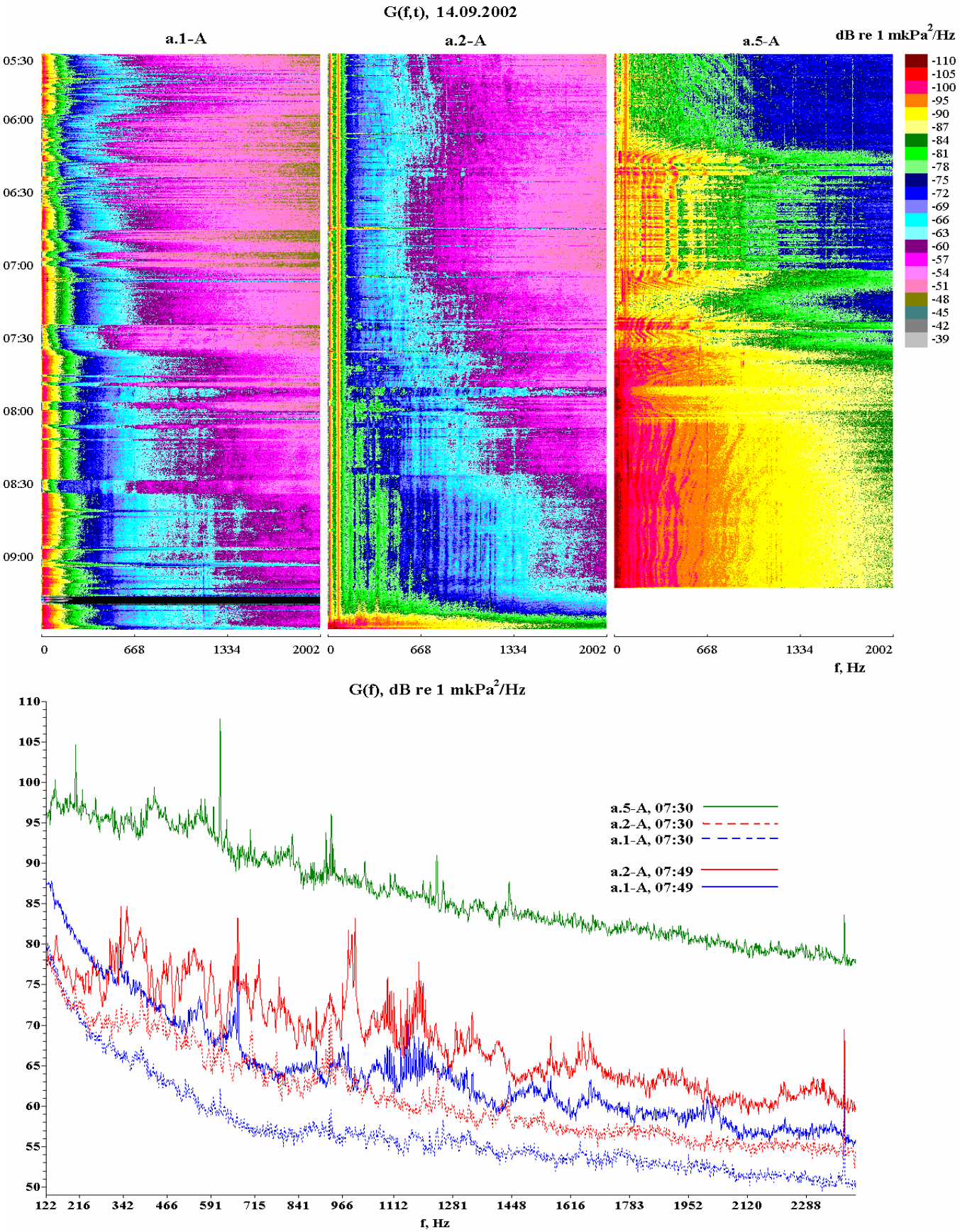

Figure 2.4 - Sonograms *G(f,t)* and spectra *G(f)* of anthropogenic acoustic noise synchronously at locations a.1, a.2 and a.5 (analog sonobuoys). This noise was monitored as the *Okha* approached the Molikpaq platform on 14 September 2002.

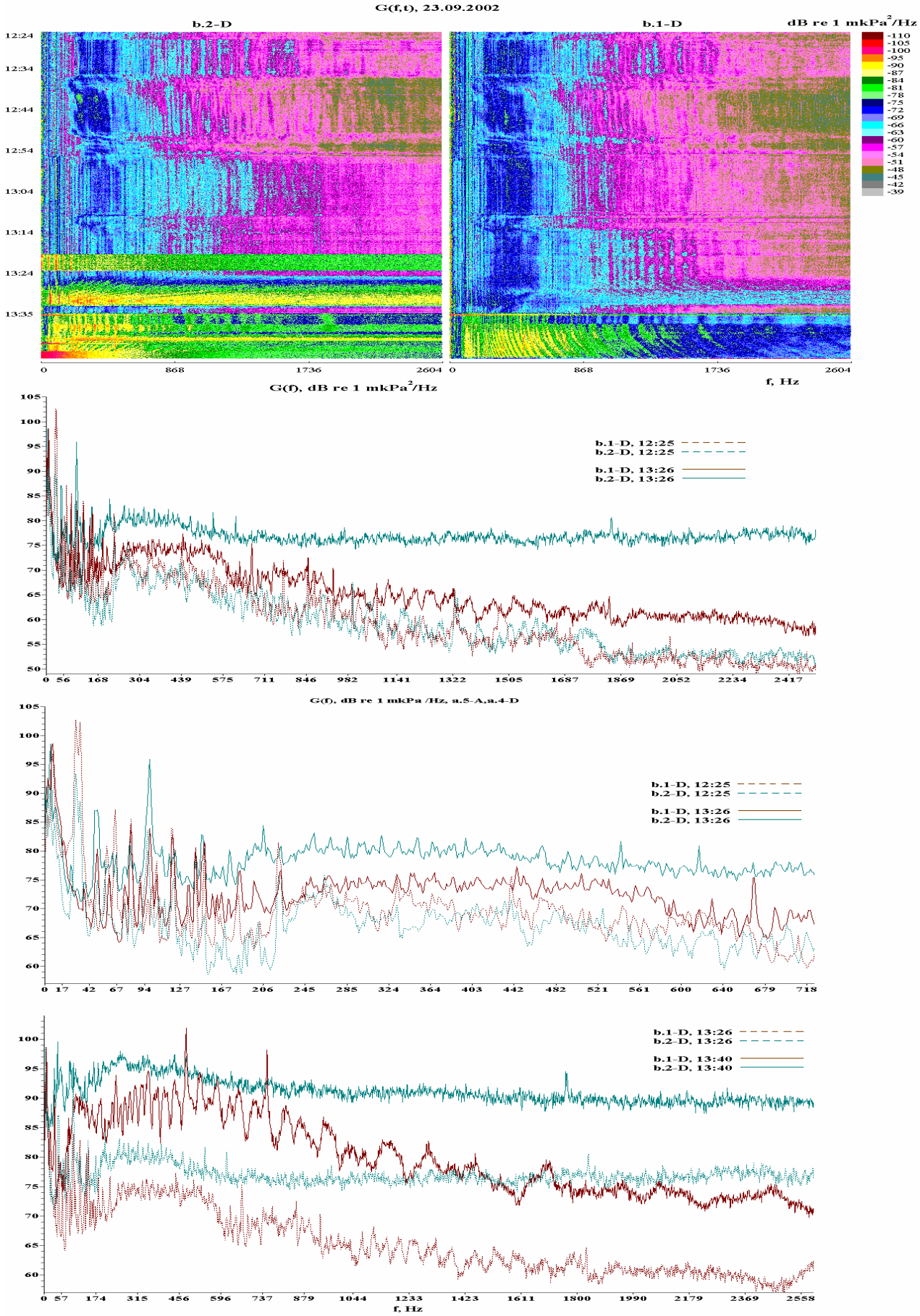

Figure 2.5 Sonograms *G(f,t)* and spectra *G(f)* of anthropogenic noise recorded at locations b.1 and b.2 (digital sonobuoys) on 23 September 2002.

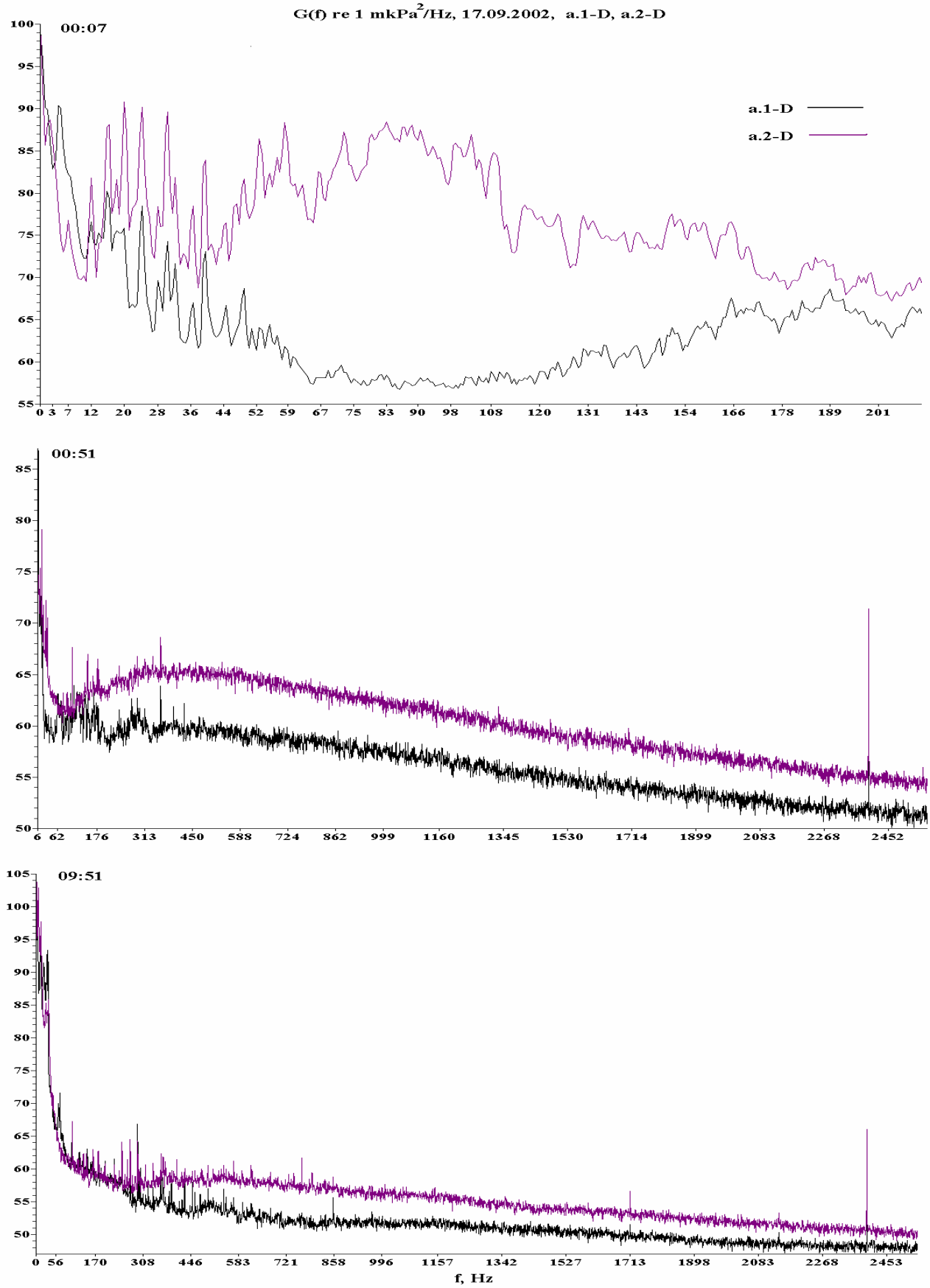

Figure 2.6 - Spectra *G(f)* of acoustic noise synchronously recorded at locations a.1 and a.2 (digital sonobuoys) on 17 September 2002.

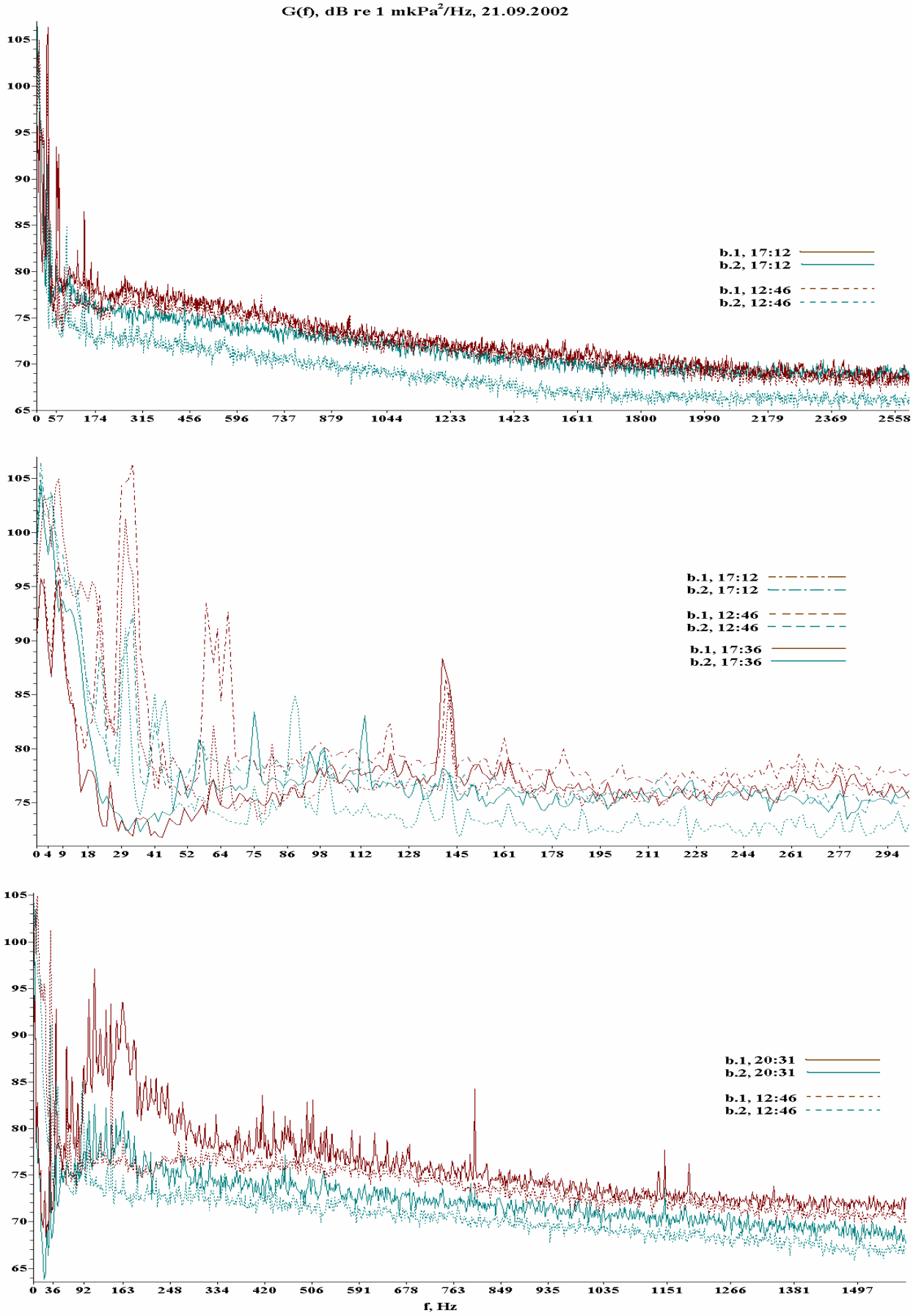

Figure 2.7 - Spectra *G(f)* of ambient noise recorded at locations b.1 and b.2 (digital sonobuoys) on 21 September 2002.

2.2 Experimental analysis of acoustic propagation in shallow water

Figure 2.8 is a map of the NE section of the Sakhalin shelf, where acoustic experiments were conducted in conjunction with the 2001 Odoptu seismic program [Borisov et al., 2002, 2003][1,2]. Acoustic data from 10 Hz to 5 kHz was recorded by three sonobuoys at locations T.4, T.5 and T.6, and by two hydrophones deployed from the vessel *Grif* with a vertical separation of 10 m. The lines show the acoustic profiles along which measurements were made. The source locations of the MV *Nordic Explorer's* air gun array are marked with 'S#' and the sonobuoy locations with 'T#'.

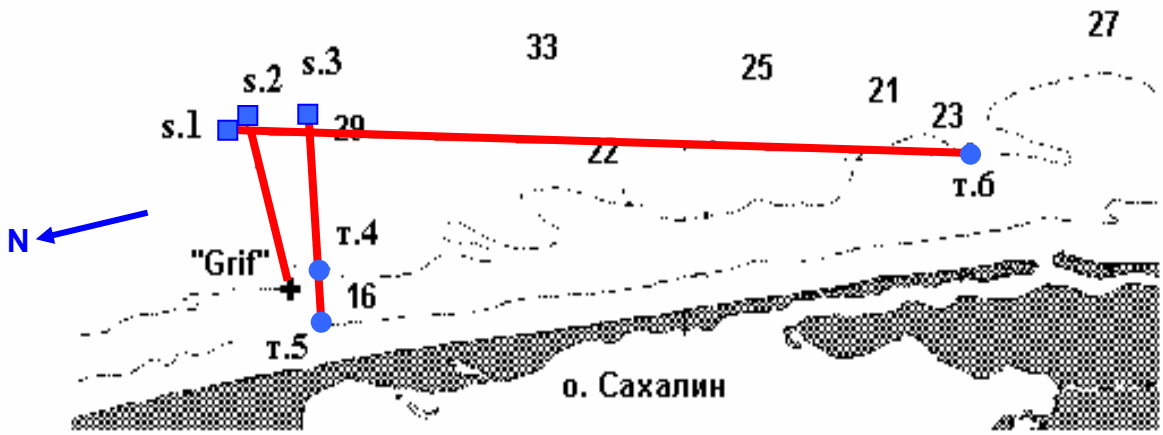

Figure 2.8 - Map showing the layout of the Transmission Loss experiments.

The results of these experiments were used to calculate the spatial and spectral *G(f)* acoustic transmission characteristics of signals generated by air guns deployed at a depth of 6 m from the MV *Nordic Explorer*. Figure 2.9 shows the time domain *A(t),* frequency domain *G(f)* and the frequency-time distribution of energy *G(f,t)*[20] from two seismic pulses.

Acoustic pressure was measured near the bottom by a hydrophone deployed from the *Grif* and on the bottom by a sonobuoy at point T.6. The seismic impulses were generated at points S.1 and S.2 (Figure 2.8); the range was 7 km to the *Grif* and 34 km to point T.6.

[20] Using the Wigner-Ville transform - the acoustic data is divided into two sections each being analyzed separately; the results are then plotted on the same sonogram. The separation time is slightly shorter than the direct arrival time, this approach can avoid contamination of the seismic wave by the water wave and vice-versa. The transform resolution was 1 Hz in frequency and 2 ms in time.

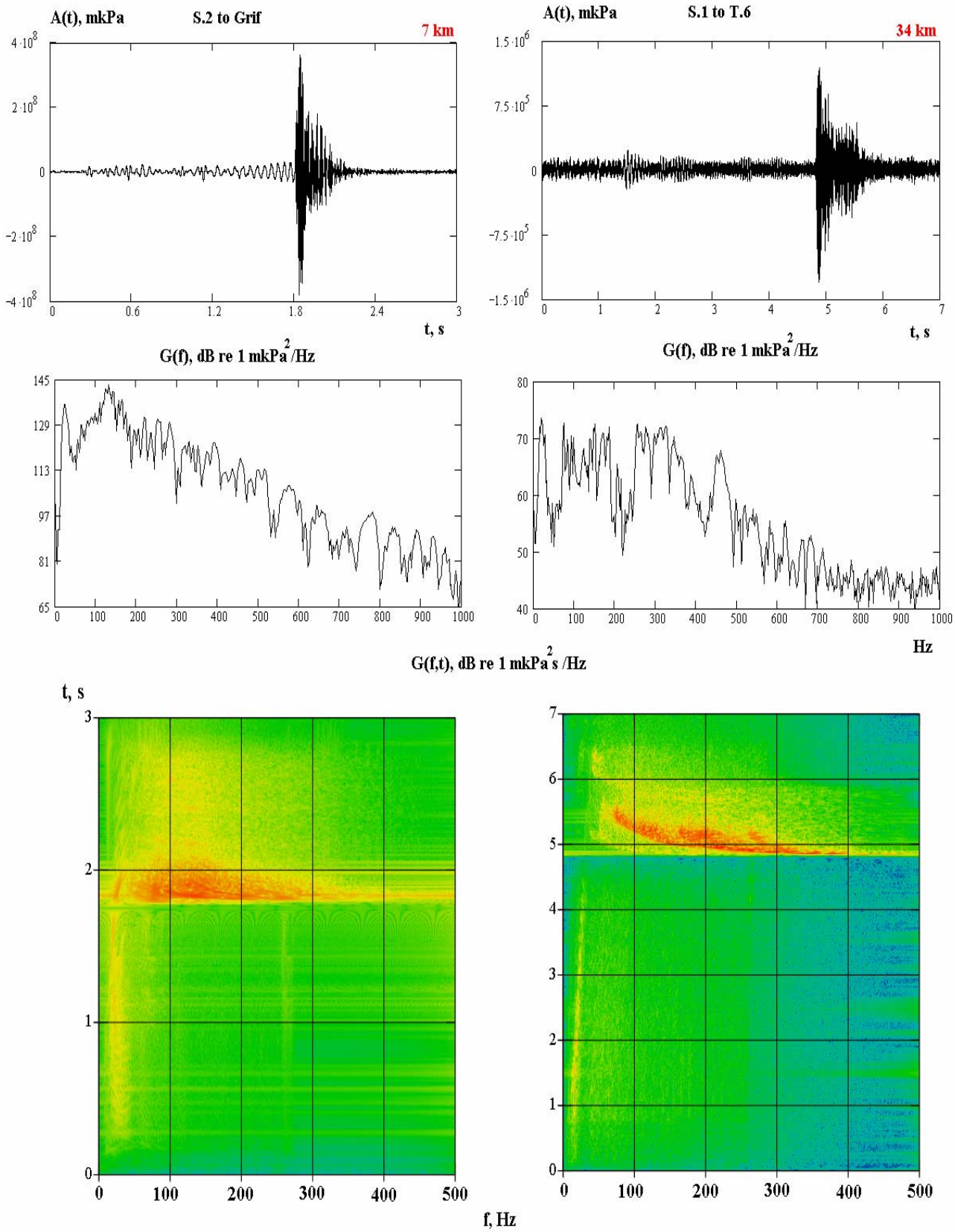

Figure 2.9 - Time domain, frequency domain and frequency-time (sonogram) plots of impulses from the *Nordic Explorer* recorded on the *Grif* and by sonobuoy T.6.

Acoustic energy propagates in the water and sub-bottom as 3 types of waves. A body wave with a high group velocity (close to earth velocity c_1), an Airy phase traveling at the minimum group velocity (lower than water velocity), and acoustic waves traveling in the water, whose group velocity varies with water depth, approaching c_0 (water velocity) at high frequencies. The spectral shape depends on the range to the source. At long ranges the major transmission path is through the earth, where the high frequencies of the acoustic signal are attenuated, this mode has a spectral peak at ~20 Hz. Most of the acoustic energy at frequencies lower than 60 Hz. (i.e. approximately the critical frequency for 20 m water depth (80 Hz)) travels through the earth.

The spectrum *G(f)* of the signal recorded at a range of 34 km (T.6) differs significantly from the shorter-range signal recorded on the *Grif* (Figure 2.9). The first arrival at T.6 is the seismic arrival with a 73 dB spectral peak at 20 Hz; this is followed by the broader band arrival through the water. However the spectral density *G(f)* levels out within the frequency band from 90 to 350 Hz, although there is a moderate drop of greater than 10 dB from 180-220 Hz, and a spectral peak at 460 Hz. This spectral distribution is caused by the specifics of the acoustic transmission in the area. The spectral *G(f,t)* plots from Figure 2.9 show the frequency-time distribution of broadband acoustic pulses propagating on the shelf. If the water velocity is assumed to be 1500 m/s, then the acoustic energy was propagating to point T.6 at ~2000 m/s (20 Hz). This figure shows clear mode dispersion with the mode structure dependent on the parameters of the waveguide.

Figure 2.10 shows spectra *G(f)* for signals propagating between shot S.3 and sonobuoys T.4 and T.5 (Figure 2.8). The depth at T.4 is 20m, at T.5 10m and the distance between T.4 and T.5 is 1.88 km. These spectra are for data synchronously recorded at locations T.4 and T.5 and show the frequency dependence of acoustic losses near the shore, as the depth decreased by 10 m the spectral density decreased by 20 dB in the 30-60 Hz frequency band. Theoretical estimates for a comparison waveguide show that the first mode of a 30 Hz acoustic wave can propagate at T.4, but the critical frequency at T.5 is 60 Hz, so energy carried by waves with frequencies lower than 60-70 Hz is absorbed by the bottom.

The modeled[21] acoustic losses between S.1 and T.6 were 82 dB, between S.2 and the *Grif* 17 dB for a differential attenuation of 65 dB. Spectral density plots *G(f)* on Figure 2.9 reveal that the spectral density difference at 20 Hz between the T.6 and *Grif* profiles is approximately 63 dB, the theoretical estimate is therefore close to the experimental result.

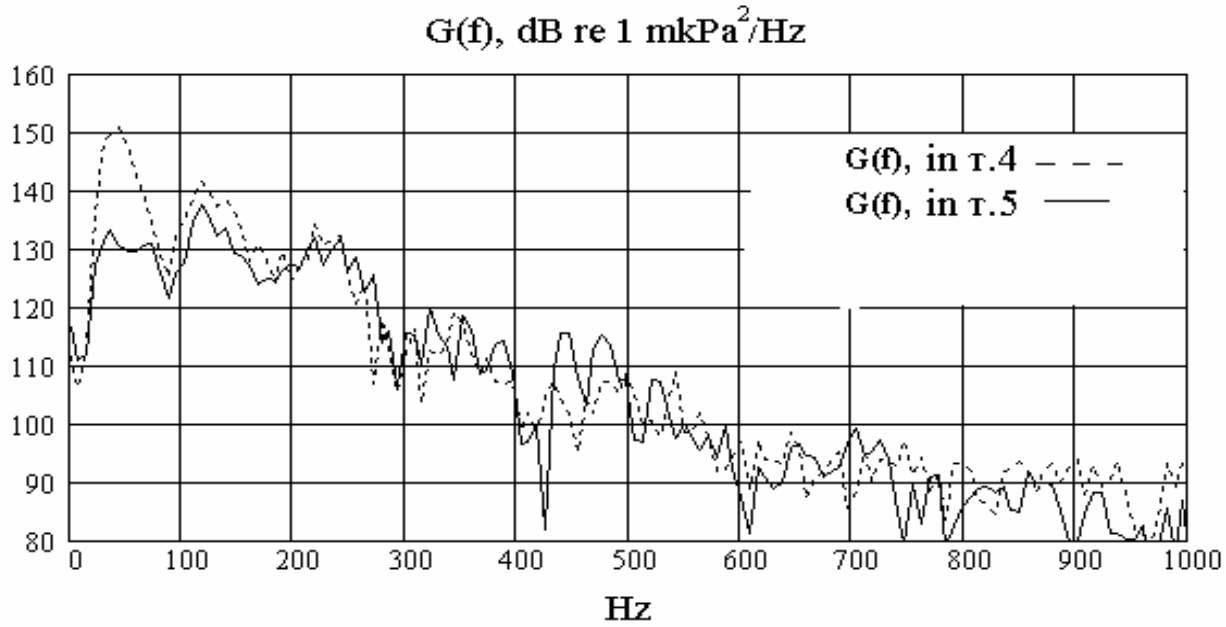

Figure 2.10 - Amplitude spectra synchronously recorded by sonobuoys at locations T.4 and T.5 (1.88 km apart).

The validity of the estimated absorption coefficient of 0.12 dB/km/Hz can be confirmed in a separate experiment. The spectral level of the narrow band (26 Hz) noise generated by the *Chara* (Figure 2.6: 00:07h) and recorded at locations a.1 and a.2 is 12 dB greater at a.1 than at a.2, at 13 Hz it is 5 dB more. The distance between the *Chara* and location a.1 is 4 km more than to location a.2 (a.1 and a.2 are 5.6 km apart). If the absorption coefficient for compressional waves in an unconsolidated layer is assumed to be 0.12 dB/km/Hz the estimated spectral difference between the two locations should be 12 dB for 26 Hz and 6 dB for 13 Hz.

When estimating acoustic propagation and attenuation, it is often more effective to average the acoustic power over a unit area (intensity) than to evaluate the fine interference structure of the acoustic field. The spatial scale used for averaging should be greater than

[21] The model assumes the absorption coefficient for compressional waves in a non-consolidated layer is 0.12 dB/km/Hz and the dominant frequency of the seismic energy is 20 Hz.

the largest scale of the normal wave interference (i.e. the largest wavelength in the waveguide). After spatial averaging, the variation caused by the interference of different modes and the interference variation with a spatial scale greater than a wavelength disappear and the relationship between the intensity and the distance to a sound source becomes smooth. This averaging is very effective if the number of modes propagating in a waveguide is large; a similar result can be obtained by averaging not in space, but in frequency[22] if the source is broadband.

Averaging by spatial interval:

$$\Lambda_l \approx 2\pi \frac{1}{|q_{l+1} - q_l|} \tag{3}$$

can help to avoid the beating caused by members such as:

$$e^{i(q_{l+1} - q_l)r} \tag{4}$$

Where:

Λ_l is the intermodal (spatial) period (the envelope of the modes). At the maximum the modes (l, l+1) are in phase at the minimum in contraphase.

q_l is the horizontal component of the propagating l_{th} mode k_l.

r is the spatial averaging distance.

When averaging by frequency, the typical frequency band is:

$$\Delta\omega \approx \frac{2\pi}{r\left[\frac{d(q_{l+1} - q_l)}{d\omega}\right]} \tag{5}$$

Thus $dq_l/d\omega \approx \omega/q_l c^2$ is equal to $\Delta\omega/\omega \approx \Lambda_l/r$ [Borodin et al., 1992].

For certain models of acoustic waveguides the relationship between averaged intensity and distance can be analytically derived. Brekhovskikh stated that for a Pekeris model[23] the intensity attenuates as $r^{-3/2}$ [Brekhovskikh, 1965], this attenuation, intermediate between cylindrical and spherical spreading, is caused by multiple reflections from the partially

[22] If a source is broad band the averaging is not to range at fixed frequency, but to frequency at fixed range.

[23] Water layer has constant velocity and density, bottom parameters are constant with partially absorbing bottom.

absorbing bottom. Katsnelson et al. described a general method for estimating the sound intensity in a waveguide with varying depth and velocity and having multiple reflections from a semi-absorbing boundary [Katsnelson et al., 1997]. For a waveguide bounded by the sea surface and an irregular water bottom (with bathymetric relief), the averaged intensity at a range r is defined by the integration of the waveguide parameters up to r. The averaging distance is defined through the average pressure of the sound field.

At small distances from the source, the intensity varies by r^{-2} (spherical spreading)[24]; as the number of excited modes becomes large, the intensity varies by $r^{-3/2}$ (bottom irregularities will increase this attenuation) which can be coupled with exponential attenuation for near-bottom modes[25]. The spatial interval for this dependence is defined by r^*, after this distance fewer than 3 modes (usually one) propagate and the attenuation becomes exponential[26]. In addition to spreading losses there are absorption losses, these vary linearly with distance and increase with increasing frequency (proportional to f^2). The exact attenuation also depends on the positions of both the source and the receiver, e.g. for a source near the surface and a receiver at long range, the averaged attenuation is $r^{-5/2}$, due to the distribution of modes near the boundaries (dipole transmission).

The transmission loss equation is defined as:

$$TL \equiv 20\log\left(\frac{\overline{p}}{\overline{p}_0}\right) \tag{6}$$

Where:

$\overline{p}$ is the average acoustic pressure at receiver (averaged over space or frequency).

$\overline{p}_0$ is the average acoustic pressure at a distance of 1 m from the source.

[24] Spherical spreading is the dominant spreading loss in a uniform medium.
[25] Modes where most of the energy travels near the sea bottom due to the velocity structure.
[26] This distance r* can be estimated either with a Pekeris model or a model of a near-bottom waveguide.

This transmission loss is composed of three terms (square brackets), each of these terms correspond to different spreading losses, each with a different relationship between acoustic intensity and distance:

$$TL = -\left[20\,\mathbf{log}(\frac{r_0}{r})\right] - \left[15\,\mathbf{log}(\frac{r_1}{r^*}) + \beta_1(r^* - r_1)\right] - \left[10\,\mathbf{log}(\frac{r^*}{r}) + \beta(r - r^*)\right] \qquad (7)$$

The first term corresponds to spherical spreading close to the source, the second to the law of 'two thirds' with additional attenuation, and the third to cylindrical spreading with additional attenuation. Equation (7) is empirical; however, the second term corresponds to the situation when a large number of modes propagate in a waveguide and the third when there are several near-bottom modes with similar attenuation coefficients. The transitional distance r_1 can be estimated with the equation:

$$r_1 \equiv \frac{H^2}{2\lambda} \qquad (8)$$

At that distance the Fresnel ray radius[27] is equal to a half of the waveguide [Kravtsov et al., 1980]. Values of r^*, β, and β_l depend on the wavelength of the acoustic signal and the waveguide parameters, including sea bottom irregularities.

Experiments designed to estimate transmission loss in a shallow sea used a vessel moving away from the receiver towing tonal, narrowband, and broadband transmitters. The sampling frequency of measurements conducted with a tonal source is greater because continuous measurements can be made as the vessel moves away towing the transmitter. The sampling distance over which discrete amplitude measurements are made is $\Delta r_d = \nu T$, where ν is the vessel speed and T is the time necessary for signal accumulation. For a vessel speed $\nu \approx 1.5$ m/s and $T \approx 50$ s the value of $\Delta r_d \approx 75$ m, this spatial sample interval is less than the typical scale of variation in the acoustic field $\Lambda_{min.}$ This is defined by the minimum beat period for intermodal interference:

$$\Lambda_{\mathbf{min}} = 2\pi\left|q_l - q_m\right|^{-1} = 2\pi\left|\sqrt{k^2 - \frac{0.56\pi^2}{H^2}} - \sqrt{k^2 - \frac{m^2\pi^2}{H^2}}\right|^{-1} \qquad (9)$$

[27] Distance at which the wavefront is well developed (becomes a planar wavefield).

As the distance increases, only few energetic modes remain and Λ_{min} increases. If $2\Delta r_d \leq \Lambda_{min,}$ then by sampling theory, the sequence of amplitude measurements and attenuation estimates adequately represent the true spatial variations.

Because the frequency dependence of propagation parameters cannot be determined using tonal signals, broadband transmitters are usually used for this task. In the field, tonal signals generated by low frequency and high frequency transducers deployed from the anchored *Irbis* were used for transmission loss measurements. Two algorithms were used to estimate Relative Transmission Loss (RTL) from experiments that used the noise generated by a moving vessel.

The first excludes the effect of normal wave interference by averaging the spectral density *G(f)* in the frequency band $(f_m; f_n)$:

Since:

$$\frac{\Delta f}{f} \rangle \frac{\Lambda_I}{r}$$

$$\Delta f = |f_m - f_n|$$

Then:

$$RTL_{average}\left[(f_n; f_m), r\right] = 10\,\mathbf{log}\left(\hat{G}_{1\mu Pa^2}(\Delta f)\right) \tag{10}$$

$$\hat{G}_{1\mu Pa^2}(\Delta f) = \frac{G_{1\mu Pa^2}(f_n) + \ldots + G_{1\mu Pa^2}(f_m)}{m - n + 1} \tag{11}$$

The second finds the maximum spectral density in the band and calculates its dependence on the range between the source and receiver (*r*):

$$RTL_{\mathbf{max}}\left[(f_n; f_m), r\right] = 10\,\mathbf{log}\left(G_{\mathbf{max};1\mu Pa^2}(\Delta f)\right) \tag{12}$$

$$G_{\mathbf{max};1\mu Pa^2}(\Delta f) = \mathbf{max}\left\{G_{1\mu Pa^2}(f_n); \ldots G_{1\mu Pa^2}(f_m)\right\} \tag{13}$$

3 Experimental analysis of sound propagation from the Molikpaq Area to Piltun Bay

Theoretical and experimental studies of the propagation of sound from the Molikpaq to the shallow area around Piltun Bay, where there is a major concentration of feeding Gray whales, have been conducted since 1999 [Sobolevsky et al. 1999, 2000].

It should be noted that TL results from theoretical models are only as accurate as the parameters used in the model. The accuracy of TL estimated from a theoretical model can vary dramatically with changes in the acoustic and elastic parameters of the model and the bathymetry. Field observations can be used to calibrate models and constrain the results. Models will therefore be used to determine possible areas of investigation, field observations will be used as a final control.

This section describes experimental studies of acoustic propagation from the Vityaz oil production complex to the mouth of Piltun Bay; the profile and sonobuoy locations are shown on Figure 3.1. The mouth of Piltun Bay is approximately opposite Piltun lighthouse, which is marked by an orange circle. Figure 3.2 shows the variation in depth along the transect constructed using the sonar on the *Irbis*. It shows that the depth profiles are complex, explaining the complicated propagation characteristics in the area and the difficulties in accurately modeling the frequency dependent TL. During the experiment, data (to 10 kHz) from the analog and/or digital sonobuoys at a.1 and a.2 were synchronously received at Piltun lighthouse. Data from the analog and/or digital sonobuoys at a.4 and a.5 as well as the calibrated transducer hydrophone G_0 were received on the *Irbis*. Simultaneous measurements of the noise levels at these four locations enable the transmission loss between the two locations to be determined.

Tonal signals generated by the HF transducer deployed from the anchored *Irbis* located at point i.3 commenced on 15 September at 00:47h, the signal level was monitored by a calibrated hydrophone[28]. During this experiment, data were recorded from analog sonobuoys at a.1 and a.2 and analog and digital sonobuoys at a.4 and a.5. The ranges from location i.3 to the sonobuoys were: a.1 - 18 km, a.2 - 12.3 km, a.4 - 1.6 km and a.5 - 2.9 km.

---

[28] The signal level from the transducer was monitored with a calibrated hydrophone (G_0) at a distance of 2 m from the transducer. 6 dB was added to the signal measured by this hydrophone to give the source level of the transducer.

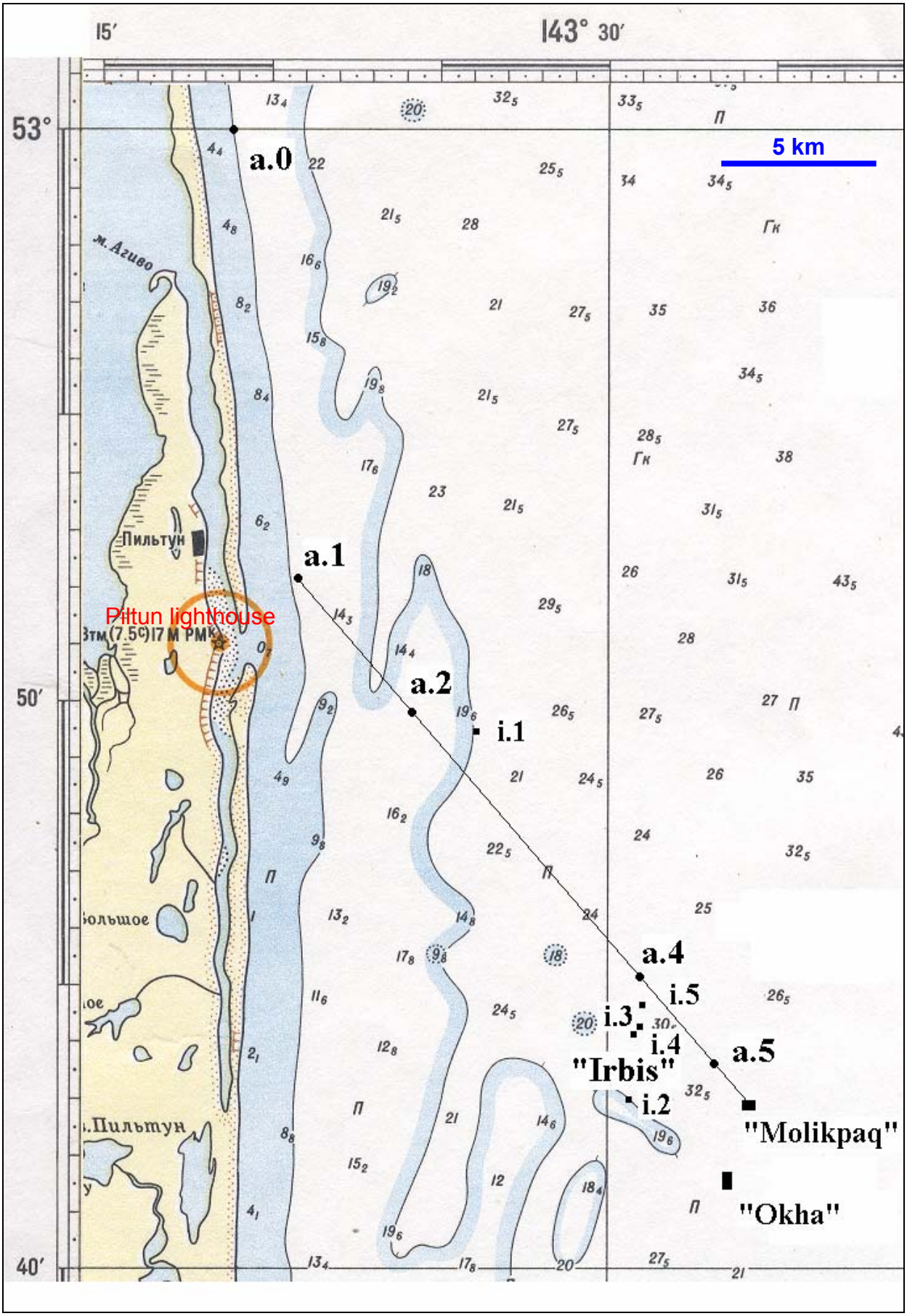

Figure 3.1 - Map of the study area showing the locations of sonobuoys (a.1 .. a.5), and the source locations (i.1 .. i.5) where the *Irbis* was located.

Table 3.1 represents TL values (re level @ 1 m) averaged in both time and space. The tonal signal was transmitted for five minutes, and since the *Irbis* had a single anchor the transducer moved over time[29].

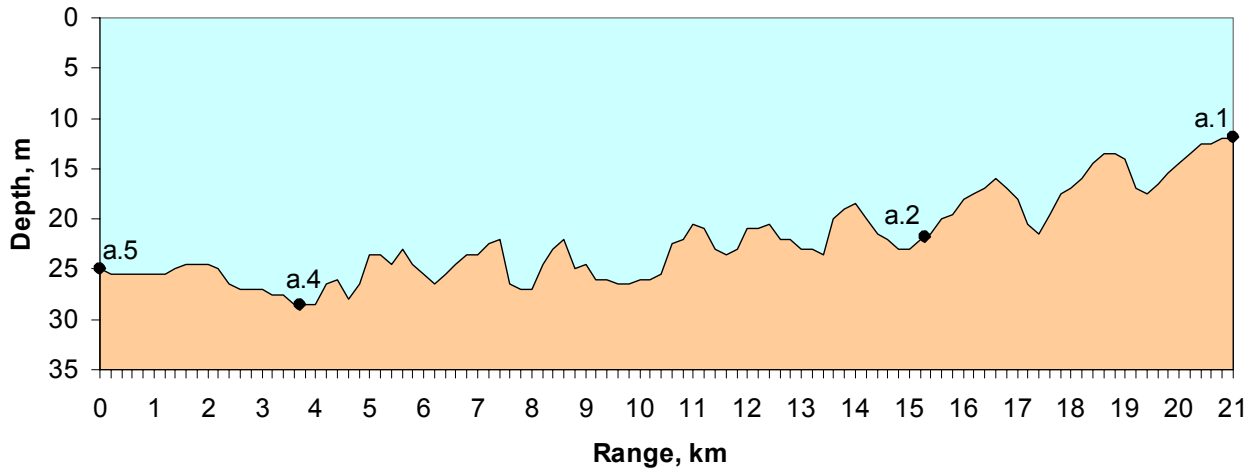

Figure 3.2 - Bathymetric profile of the study area showing the locations of sonobuoys a.1, a.2, a.4 and a.5.

Table 3.1 - TL estimates from the 15 September 2002 experiment.

	a.4	a.5	a.2	a.1
Hz.	**TL (dB)**	**TL (dB)**	**TL (dB)**	**TL (dB)**
9000	-59	-74		-104
8000	-54	-71	-89	-96
7000	-50	-65	-80	-83
6000	-46	-64	-81	-83
5000	-55	-62	-84	-86
4000	-56	-61	-81	-85
3500	-52	-61	-83	-87
3000	-50	-60	-77	-82
2500	-53	-63	-83	-85
2000	-54	-66	-79	-83
1500	-54	-67	-79	-82
1000	-52	-63	-74	-79
	Range: 1.6 km	*Range: 2.9 km*	*Range: 12.3 km*	*Range: 18.0 km*

[29] The data from a.4 and a.5 had additional spatial averaging for signals with frequencies lower than 2.6 kHz as measurements were taken with an analog and digital sonobuoy simultaneously.

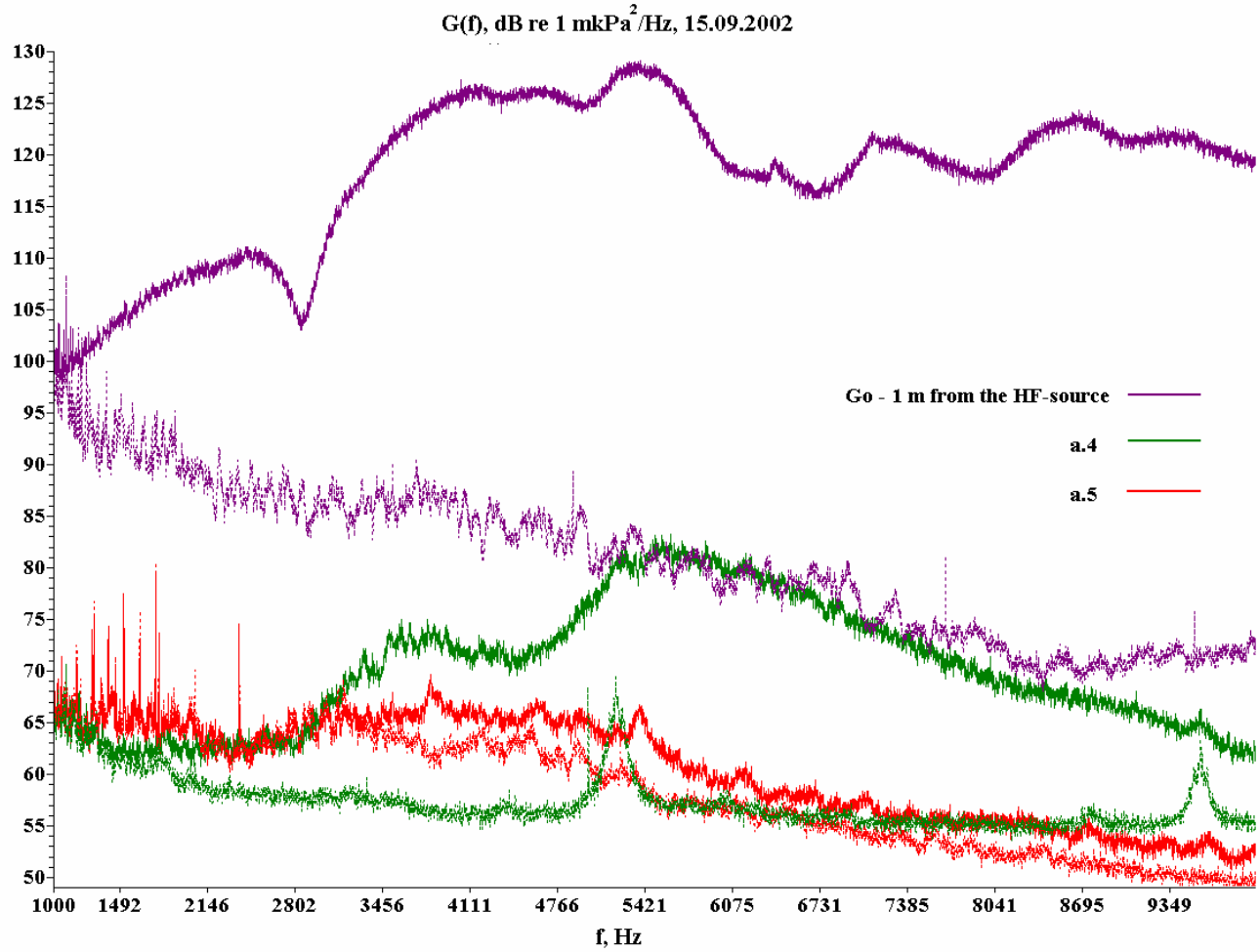

Figure 3.3 - Spectra *G(f)* of HF data recorded synchronously from a reference hydrophone plus analog sonobuoys at locations a.4 and a.5.

This averaging in time (and space due to the motion of the source) eliminates the error caused by spatial interference. The level of a transmitted tonal signal depends on its frequency so the TL in the table is relative to its level at a distance of 1 m from transmitter. Figure 3.3 shows the TL characteristics at a distance of up to 3 km from the source, the solid lines on the spectral density *G(f)* plot correspond to the time when the transducer was actively transmitting a signal[30], the dotted lines to a time when the transducer was not operational. The plot of G_0 represents the power spectrum of the acoustic field measured at a distance of 2 m from transducer and corrected to 1 m, this spectrum shows the frequency

[30] In this case a signal with a pseudo white noise spectrum was input at the linear power amplifier.

dependence of the broadband (1-10 kHz) acoustic field generated at point i.3. The spectral density plots for locations a.4 and a.5 estimate the frequency dependent transmission losses of sound propagating to locations a.4 (distance 1.6 km) and a.5 (2.9 km).

Table 3.2 - TL estimates from the 16 September 2002 experiment.

	a.4	a.5	a.2	a.1
Hz	**TL (dB)**	**TL (dB)**	**TL (dB)**	**TL (dB)**
9000	-68	-66		-111
8500	-68	-66	-100	-108
8000	-64	-61	-97	-108
7500	-60	-56	-90	-98
7000	-56	-56	-87	-95
6500	-59	-58	-87	-94
6000	-60	-60	-89	-95
5500	-62	-60	-91	-99
5000	-63	-61	-90	-96
4400	-62	-62	-94	-99
4000	-62	-63	-92	-93
3500	-67	-62	-87	-93
3000	-61	-66	-79	-83
2400	-63	-62	-83	-85
2000	-62	-63	-86	-90
1600	-65	-65	-83	-88
1250	-63	-59	-78	-81
1000	-67	-56	-73	-76
700	-60	-62	-69	-72
	Range: 2.7 km	*Range: 2.4 km*	*Range: 13.7 km*	*Range: 19.2 km*

For location a.4, the frequency dependence of the losses reaches a minimum at 5700 Hz (peak in the spectrum), this result is similar to that obtained using tonal signals and displayed in Table 3.1. The losses to location a.5 (2.9 km) have no such clear frequency dependence. These results can be explained by waveguide propagation, Equation (8)

shows that the transitional distance for frequencies between 3-9 kHz is approximately 0.9-2.7 km (for the water depths at locations a.4 and a.5). Additionally, there are a limited number of energy carrying modes, so the sound field has the frequency interference structure visible on the spectral density plot for location a.5.

The experiment with the HF transmitter was repeated on the evening of 16 September 2002. Acoustic signals were measured with analog and digital sonobuoys at locations a.1 and a.2 as well as an analog sonobuoy at location a.5. The *Irbis* was anchored at location i.4 and the ranges from i.4 to the sonobuoys were a.1-19.2 km, a.2-13.7 km, a.4-2.7 km and a.5-2.4 km. The results of this TL experiment are given in Table 3.2.

Experiments were also conducted with a LF transducer deployed at a depth of 8 m from the *Irbis* when anchored at location i.5. The ranges from location i.5 to the sonobuoys were a.1-17.4 km, a.2 - 12.1 km and a.5 - 3.3 km. Only one mode of 20-30 Hz acoustic energy can propagate in a 25 m deep waveguide, the low frequency transmission loss can therefore be estimated with tonal signals. Experiments with a similar transducer (CW-32) on the shelf of the Sea of Japan [Borisov et al., 1996], reveal that the intensity of the acoustic field generated by the transducer is greatly dependent on the bottom parameters[31]. Acoustic data was recorded synchronously at locations a.1, a.2 and a.5, for both 28 Hz (CW-28) and 29 Hz (CW-29) continuous wave signals; during the experiment the sea state was 4.

Table 3.3 - TL estimates[32] from the LF experiment.

	a.5		**a.2**		**a.1**	
Hz	**dB[33]**	**TL (dB)**	**dB**	**TL (dB)**	**dB**	**TL (dB)**
28	108	≈ -70	91	≈ -87	86	≈ -92
29	107	≈ -71	97	≈ -81	83	≈ -95
	Range: 3.3 km		*Range: 12.1 km*		*Range: 17.4 km*	

[31] The harder the sea floor at the sound generation point the greater the acoustic energy produced.
[32] Approximate rather than exact TL levels are given in Table 3.3 as the source level of the HF transducer is an estimate rather than a synchronous recording.
[33] dB re 1 $\mu Pa^2/Hz$

Figure 3.4 - Spectra *G(f)* of LF data recorded synchronously on sonobuoys at locations a.1 (digital), a.2 and a.5 (analog).

Figure 3.4 depicts spectra *G(f)* of data recorded at different phases of the LF experiment. Spectral levels measured simultaneously are presented in Table 3.3[34]. The results of the three Molikpaq-Piltun TL experiments presented in Tables 3.1, 3.2 and 3.3 are displayed on Figure 3.5 with axes of TL and range (r).

Table 3.4 - Regression results from Molikpaq-Piltun data.

f (Hz)	r_l (km)	r^* (km)	β_l (dB/km)	β (dB/km)	$\sqrt{D(f)}$ (dB)
28	0.00583	-	-	2.79	11.4
29	0.00604	-	-	2.75	11.1
1000	0.208	7.5	0.00913	0.240	3.95
2000	0.417	8.1	0.536	0.662	3.80
3000	0.625	7.5	0.106	0.365	5.19
4000	0.833	8.25	0.551	0.851	5.21
5000	1.142	8.5	0.586	0.971	5.41
6000	1.250	8.5	0.509	0.705	8.10
7000	1.485	8.5	0.412	0.663	8.26
8000	1.667	9.05	1.318	1.584	4.99
9000	1.875	10.25	1.653	1.757	3.10

A linear regression was conducted on the data acquired in the experiments using Equation (7). The objective of the regression was to estimate β_1 and β using a known r^* and r_1, minimizing the mean square deviation from regression data.

$$TL = \begin{cases} -20\log(r) & ; r \le r_1 \\ -15\log(r) - 5\log(r_1) - \beta_1(r - r_1) & ; r_1 < r \le r^* \\ -10\log(r) - 5\log(r_1) - 5\log(r^*) - \beta_1(r^* - r_1) - \beta(r - r^*) & ; r^* < r \end{cases}.$$

Regression has physical meaning only for very narrow limits of r^* (here 7-10 km). Physically, this means that the attenuation coefficients are positive, so the amplitude decreases with distance. Thus, this analysis is not only an estimate of exponential attenuation, but also an estimate of the distance at which only the first mode remains.

[34] Unfortunately the signal from the reference hydrophone was overwritten in error. However, as the signal level of the transducer was being adjusted on the *Irbis* it was measured as 170 dB re 1 μPa^2/Hz-2m, the

Table 3.4 gives values for β_1, β, r^*, and r_1, as well as the square root of the deviation of the experimental data from the regression function D, all these parameters were computed for the specified frequency (f). The table shows that at low frequencies the attenuation coefficients are high, this corresponds to exponential attenuation[35]. Figure 3.5 presents the results of the regression. The plots show strong exponential attenuation at low frequencies and an increase in attenuation at higher frequencies.

For a range r(m):

$$D_f = \frac{1}{M}\sum_{m=1}^{M}\left[TL_{Measured[r(m)]} - TL_{Regression[r(m)]}\right]^2 \qquad (14)$$

Where:

M is the number of ranges at which measurements were taken.
r(m) is the range from the sound source to the measurement point (# m).

For a frequency of 28 Hz Table 3.4 gives a value for β of 2.79 dB/km; this corresponds to a bottom absorption of ~0.1 dB/km/Hz. This value is close to the value of 0.12 dB/km/Hz estimated in section 2.2; this can be explained by the fact that the majority of the profile was in deep water unlike Odoptu or Chayvo.

Thus, for frequencies less than 30 Hz the TL along the profile from Molikpaq to Piltun can be approximated by the equation:

$$TL = -10\log(r) - 10\log(r_1) - \beta(r - r_1) \qquad (15)$$

For frequencies of 28-29 Hz r_1 is approximately 6 m.

---

estimated source signal level (after spherical spreading correction) is therefore 176 dB re 1 μPa^2/Hz-m.
[35] Since low frequencies propagate as a single mode the -15log(*r*) term is excluded from the regression for low frequencies.

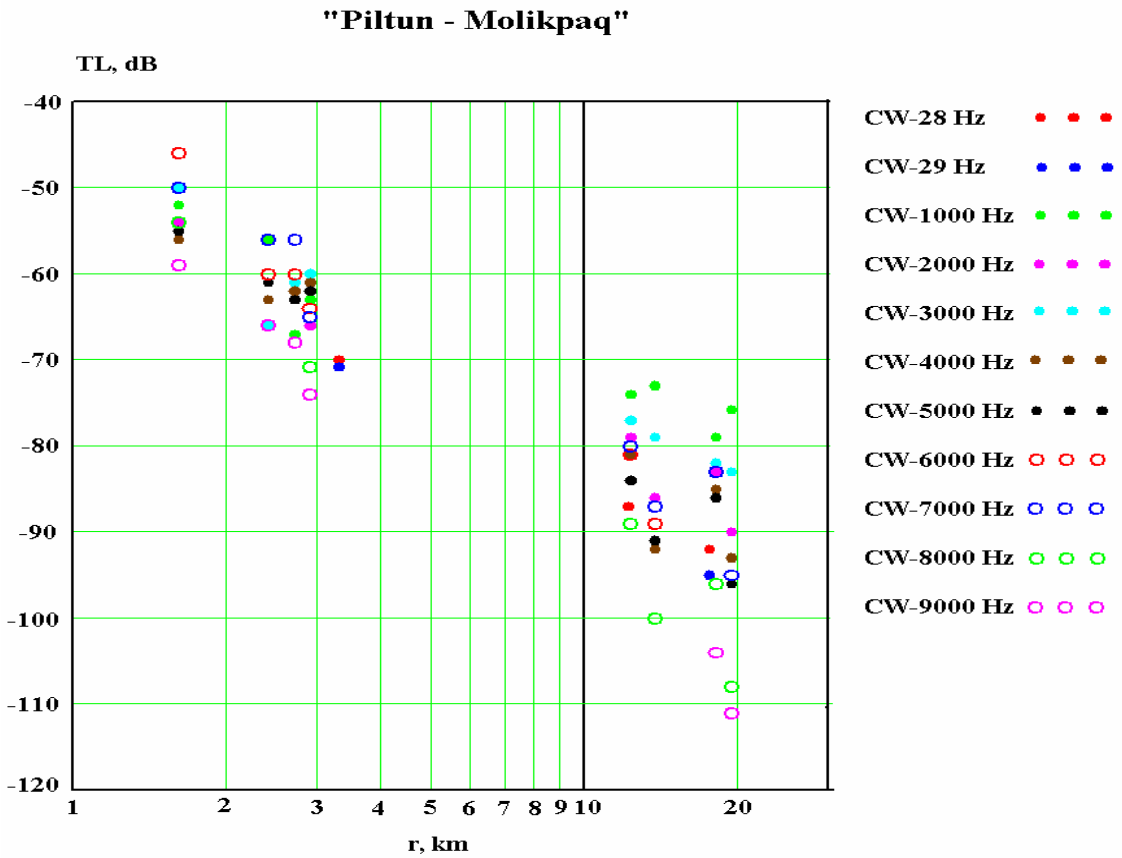

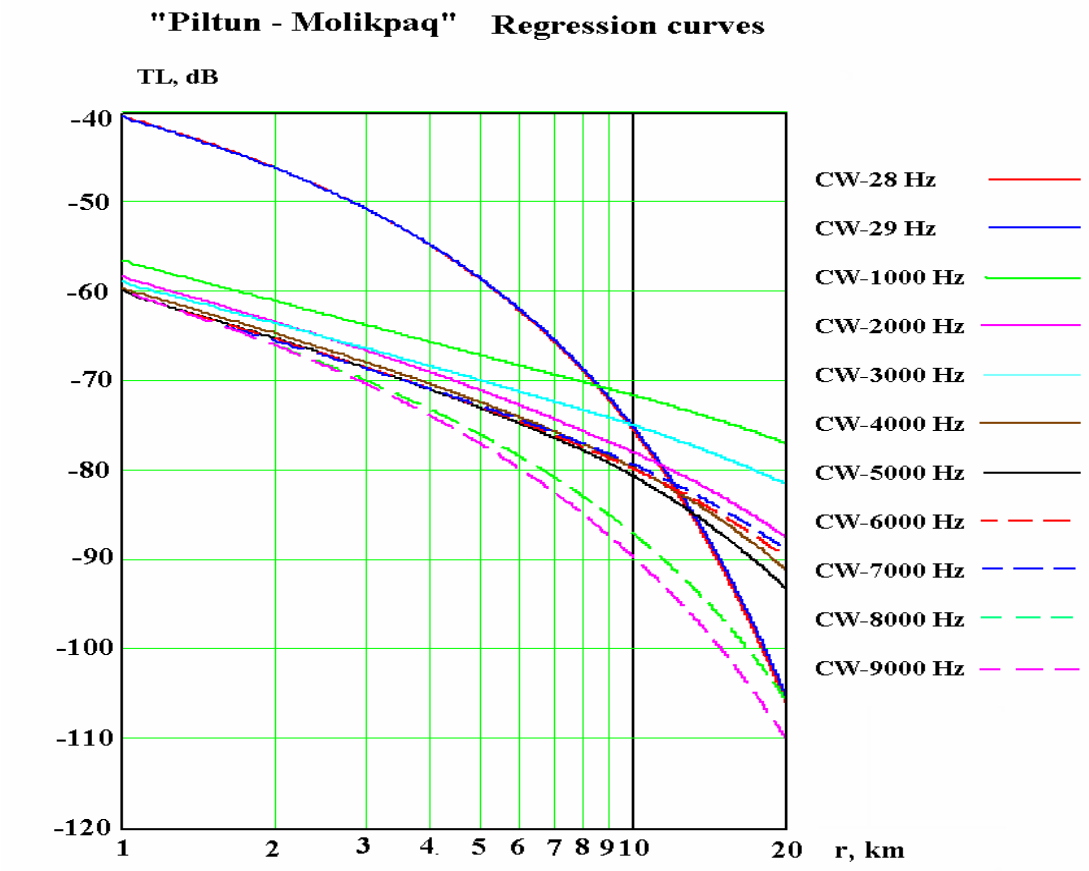

Figure 3.5 - Regression results from the Molikpaq-Piltun Transmission Loss experiments.

4 Experimental analysis of sound propagation seaward of the Chayvo area

In 2001, a new gray whale summer feeding area was discovered in water depths of 25-40 m approximately 20 km to the east of the mouth of Chayvo Bay. This section describes experimental studies of acoustic propagation from the Chayvo area to this offshore feeding area. The profile and sonobuoy locations are shown on Figure 4.1, Figure 4.2 shows the variation in depth along the transect.

A high frequency transducer deployed at 15 m depth from the anchored *Irbis* was used to investigate tonal signal propagation in the Chayvo area, the TL experiment was conducted between 9:05 and 10:20 on 22 September 2002. Figure 4.1 shows the locations b.1, b.2 and b.3 where the sonobuoys were deployed and the signals were received, the location of the transducer is marked by the word *Irbis*. A monitor hydrophone was used to measure the transmitted signal level at a distance of 1 m from the transducer. Table 4.1 presents the TL results estimated from this tonal signal experiment.

Table 4.1 - TL estimates from the 22 September 2002 experiment.

	b.1	**b.2**	**b.3**
Hz	**TL (dB)**	**TL (dB)**	**TL (dB)**
9900	-81	-71	
9000	-79	-64	-84
8000	-66	-54	
7000	-67	-56	-80
6000	-58	-49	-80
5000	-62	-54	-82
4500	-64	-63	-90
3500	-64	-59	-85
3000	-61	-56	-81
2400	-64	-55	-80
2000	-61	-57	-79
1500	-59	-59	-76
1000	-54	-54	-71
750	-56	-53	-68
	Range: 4 km	*Range: 1.8 km*	*Range: 8 km*

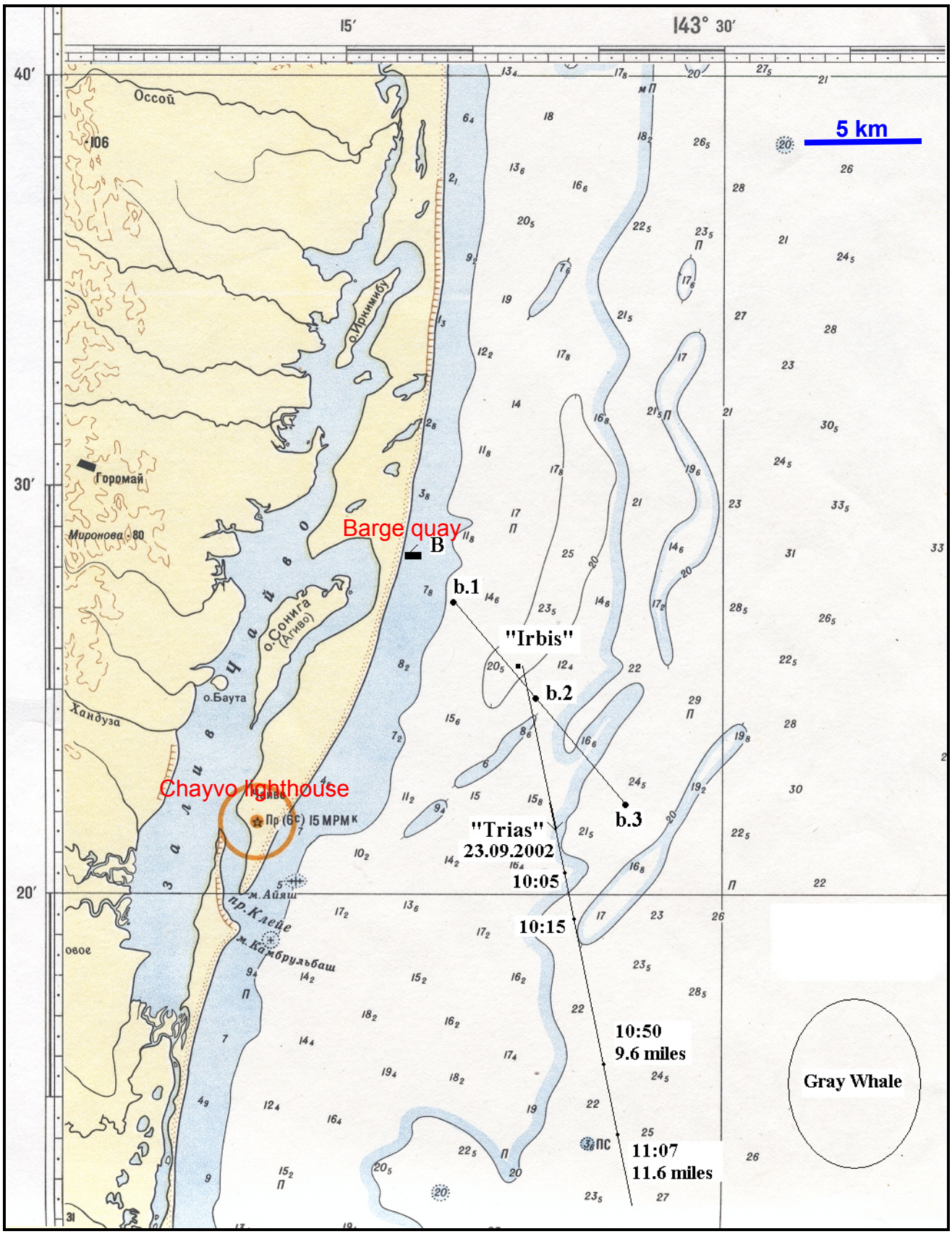

Figure 4.1 - Map of the study area showing the locations of sonobuoys (b.1, b.2 and b.3) and the source locations for the *Irbis* as well as an approximate location for the offshore gray whale feeding area.

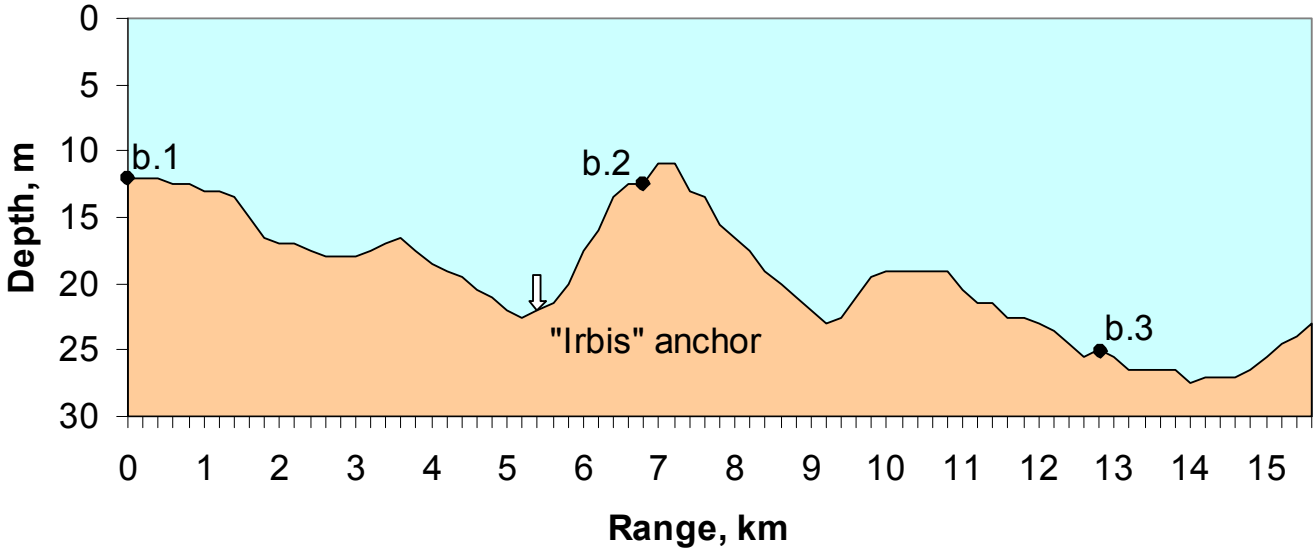

Figure 4.2 - Bathymetric profile of the study area showing the locations of sonobuoys (b.1, b.2 and b.3) and the *Irbis*.

On 21 and 22 September 2002, the *Irbis* conducted HF & LF TL experiments using a low frequency transducer deployed at a depth of 8 m, and a HF transducer at a depth of 15 m, the *Irbis* was anchored at the same location for both experiments. A monitor hydrophone was used to measure the transmitted signal level at a distance of 2 m from the transducer, 6 dB was therefore added to the measured signal level to correct to a distance of 1 m. Periodically the transducer was deliberately switched into clipping mode (meander mode) generating high harmonics. The solid lines on the spectral density *G(f)* plot (Figure 4.3) correspond to the time when the transducer was actively transmitting a signal, the dotted lines to a time when the transducer was not operational. Table 4.2 displays the results of the transmission loss measurements estimated from low and high frequency sounds propagating from the *Irbis* to locations b.1, b.2 and b.3. The results of the Chayvo TL experiments presented in Tables 4.1 and 4.2 are displayed on Figure 4.4 with axes of TL and range (r).

On the morning of 23 September the tug *Trias* departed from the anchored *Irbis* at 9:10 and sailed with approximately constant speed along a track shown on Figure 4.1, the *Trias* coordinates were periodically monitored by radar. The noise generated by the departing *Trias* was simultaneously recorded at locations b.1, b.2 and b.3 (Figure 4.5) and the data was processed through Equations (10) and (12) to average out interference effects. Point intensity measurements were computed for all three sonobuoys; these estimates were

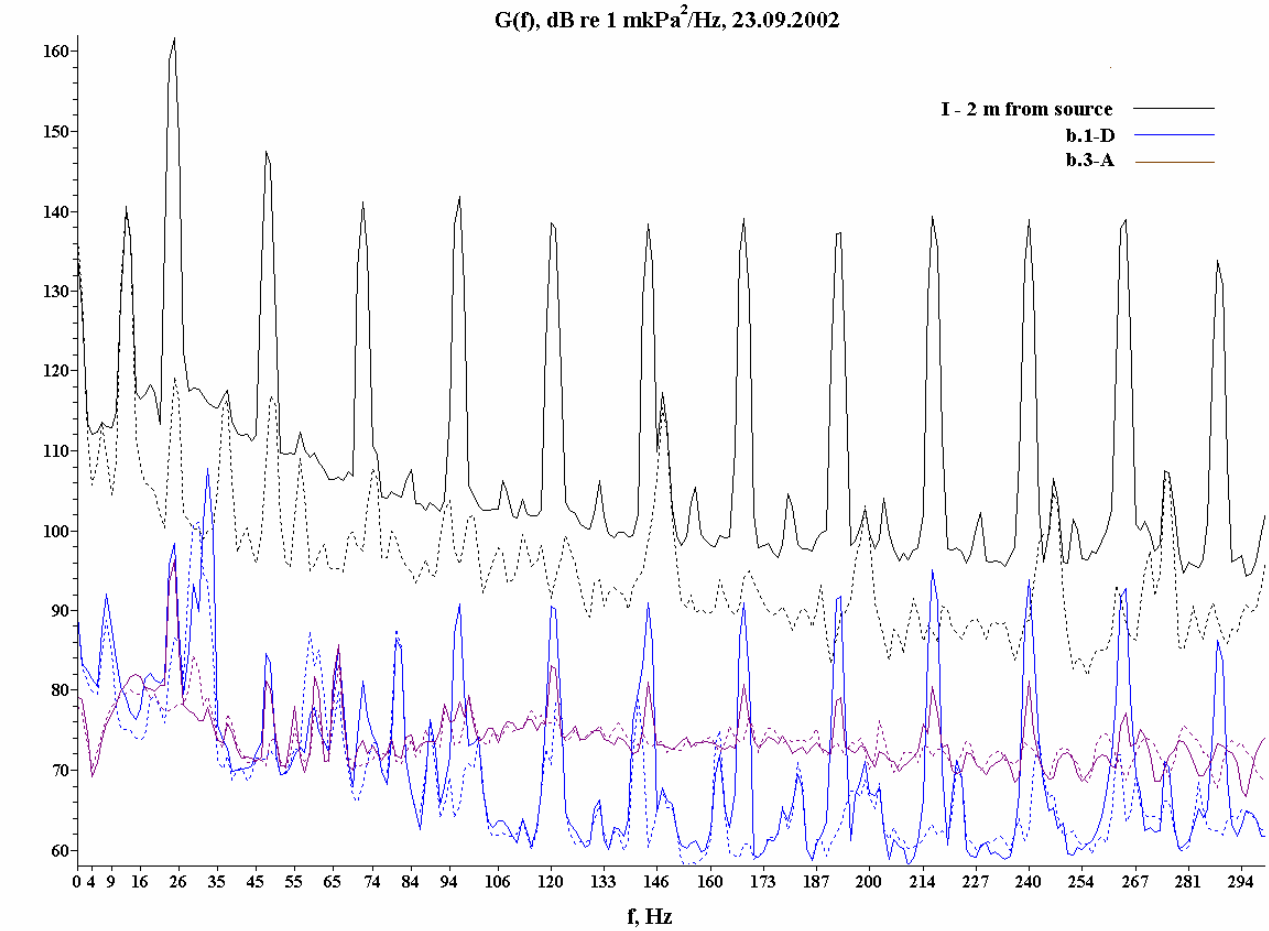

Figure 4.3 - Spectra *G(f)* of low frequency (24 Hz and harmonics) data recorded synchronously on a reference hydrophone 2 m from the transducer and sonobuoys at locations b.1 (digital), and b.3 (analog).

calculated using Equations (10) (RTL_{max}) and (12) ($RTL_{average}$) over the specified bandwidth. The time relationship was converted to a distance relationship, allowing the variation in received power with range over the specified bandwidth to be estimated. Absolute TL estimates cannot be made because the source was significantly larger than 1 m and the reference amplitude is unknown. However, the relative variation in TL (RTL) with range can be estimated from this data (Figures 4.6 to 4.8). Figure 4.6 (center) displays plots of RTL_{max} [325:725 Hz], which show relatively stable interference structures whose spatial scale increased (Δ from 200 m to 500 m, b.1 plot), but modulation depth decreased ($\delta I = I_{max} - I_{min}$ from 12 dB to 5 dB) when the *Trias* was moving away. At low frequencies (200-300 Hz) and high frequencies (1100-1930 Hz) (top and bottom plots Figure 4.6) there is no such spatial interference, since at low frequencies the propagating energy is concentrated in the low mode while at high frequencies a large number of modes are interfering.

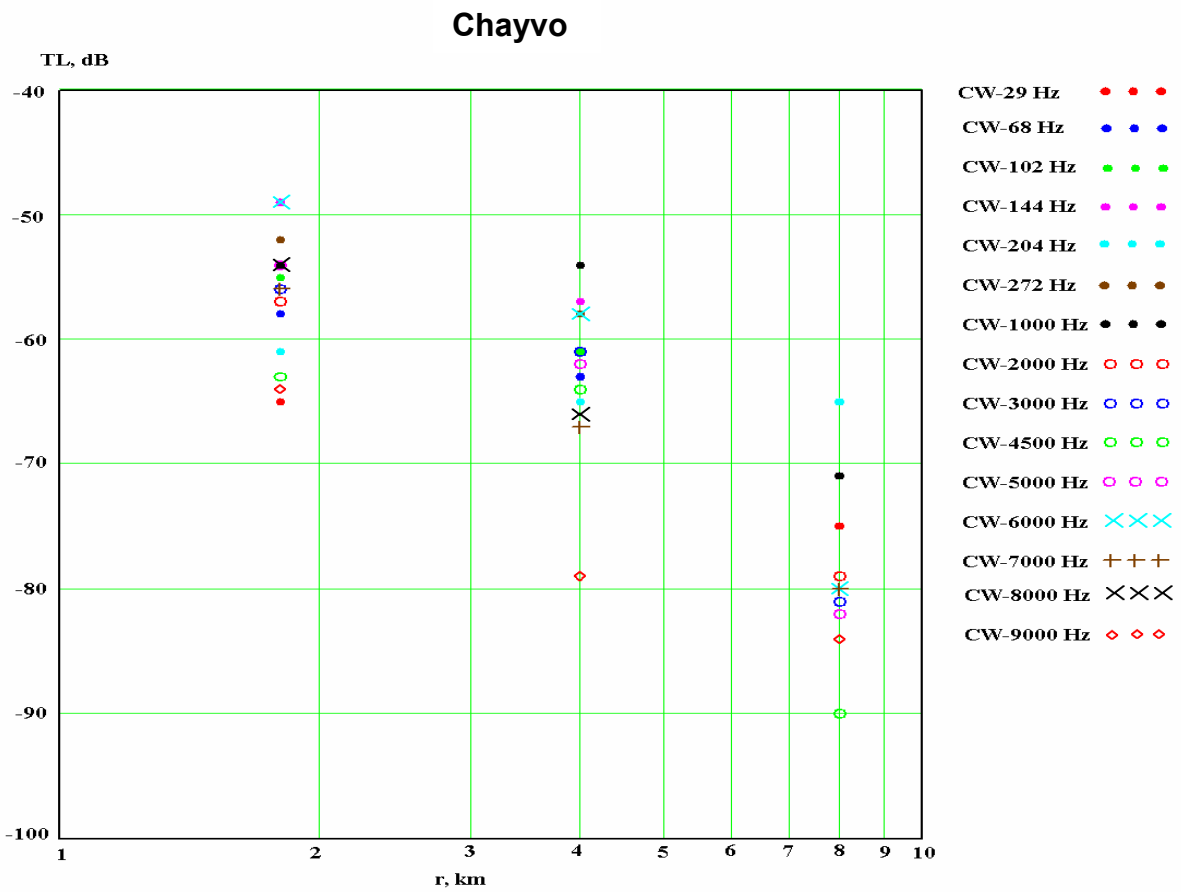

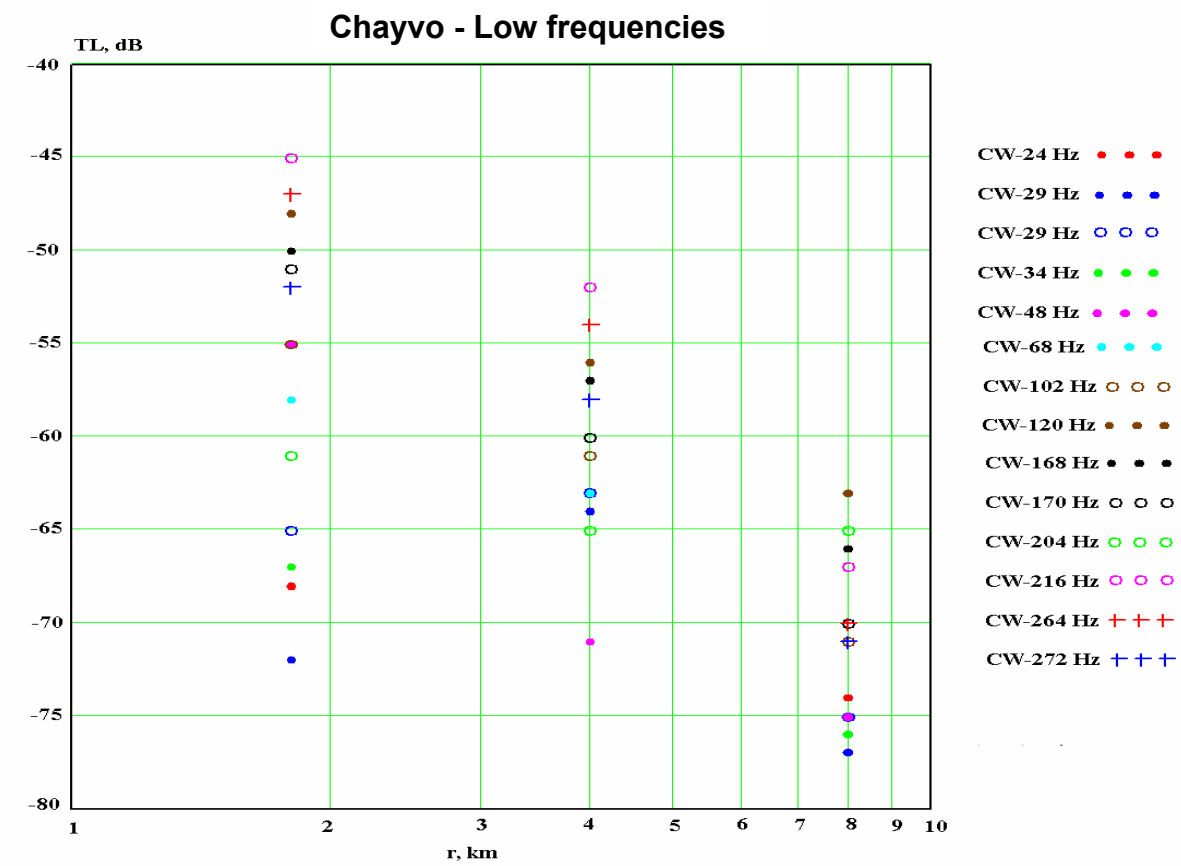

Figure 4.4 - Regression results from the Chayvo Transmission Loss experiments.

Table 4.2 - TL estimates from the 21 and 22 September 2002 experiments (resonant tones and harmonics).

	b.1	b.2	b.3
Hz	**TL (dB)**	**TL (dB)**	**TL (dB)**
29 (21.09.02-14:04)	64	72	77
29 (21.09.02-14:19)	65	74	76
33 (21.09.2002-14:32)	66	72	78
34 (21.09.2002-14:38)	63	67	76
68 (21.09.2002-14:38)	63	58	
102 (21.09.2002-14:38)	61	55	71
136 (21.09.2002-14:38)	51	49	66
170 (21.09.2002-14:38)	60	51	70
204 (21.09.2002-14:38)	65	61	65
238 (21.09.2002-14:38)	55	54	62
272 (21.09.2002-14:38)	62	57	72
34 (21.09.2002-14:44)	64	69	78
238 (21.09.2002-14:44)	57	53	71
272 (21.09.2002-14:44)	58	52	71
29 (23.09.2002-10:30)	63	65	75
87 (23.09.2002-10:30)	60		69
116 (23.09.2002-10:30)	52		62
145 (23.09.2002-10:30)	54		62
174 (23.09.2002-10:30)	53		62
203 (23.09.2002-10:30)	52		62
232 (23.09.2002-10:30)	49		64
261 (23.09.2002-10:30)	50		70
24 (23.09.2002-11:01)	73	68	74
48 (23.09.2002-11:01)	71	55	75
120 (23.09.2002-11:01)	56	48	63
144 (23.09.2002-11:01)	57	49	65
168 (23.09.2002-11:01)	57	50	66
192 (23.09.2002-11:01)	53	43	66
216 (23.09.2002-11:01)	52	45	67
240 (23.09.2002-11:01)	54	63	66
264 (23.09.2002-11:01)	54	47	70
	Range: 4 km	*Range: 1.8 km*	*Range: 8 km*

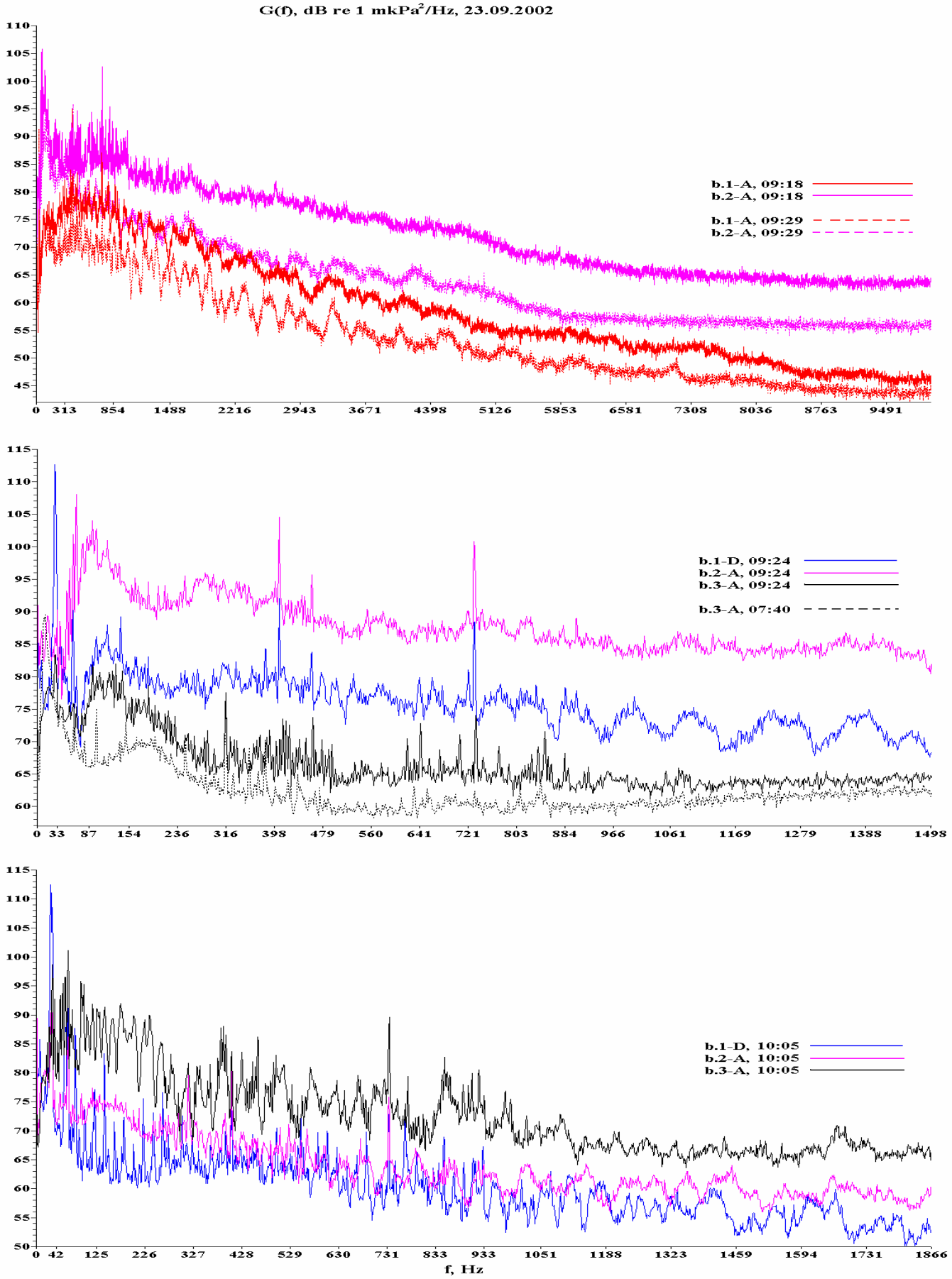

Figure 4.5 - Spectra *G(f)* of ambient and anthropogenic noise recorded at locations b.1, b.2 and b.3 (analog and digital sonobuoys) on 23 September 2002.

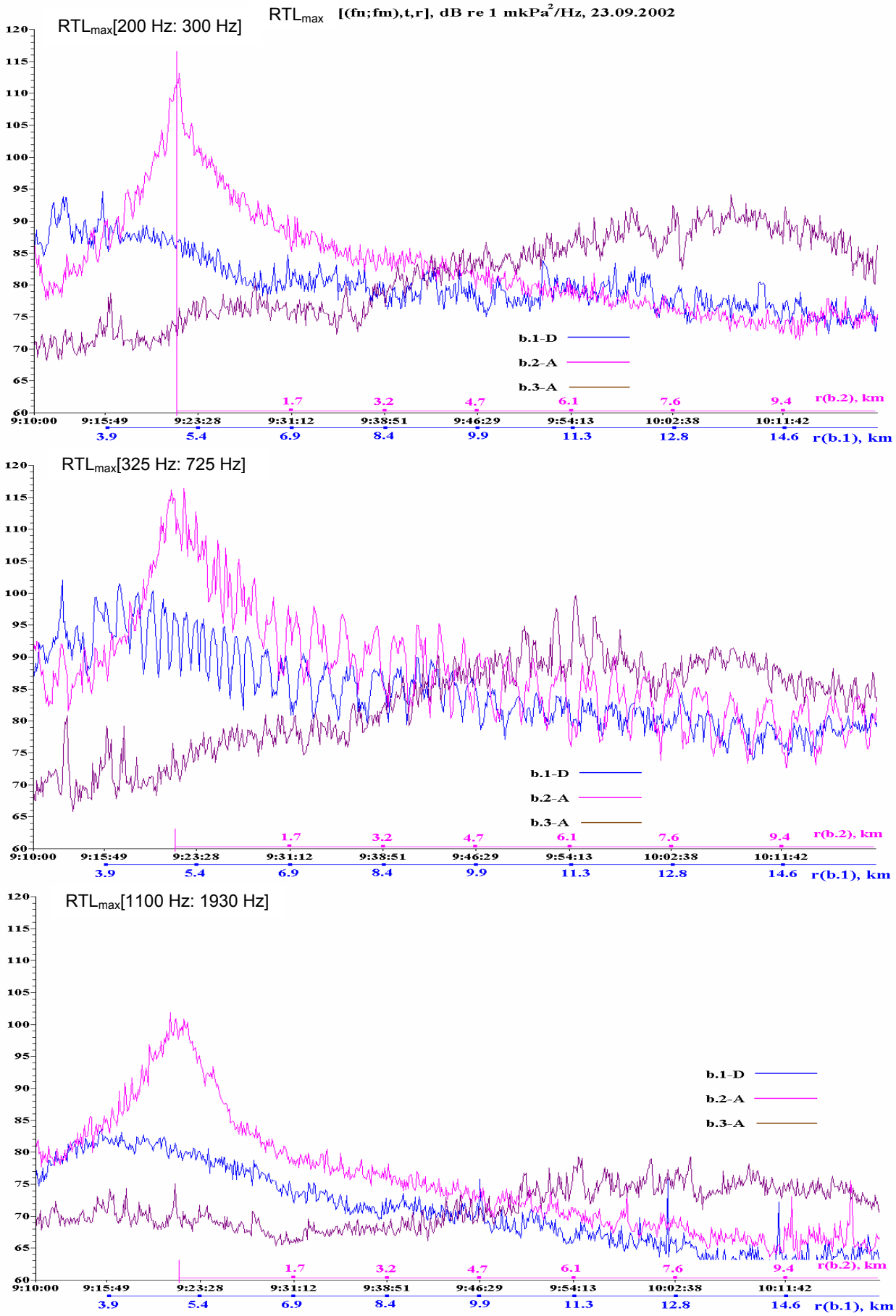

Figure 4.6 - Plots of RTL_{max} calculated with Equation (12) using noise generated by the *Trias* and recorded on sonobuoys b.1, b.2 (digital), and b.3 (analog).

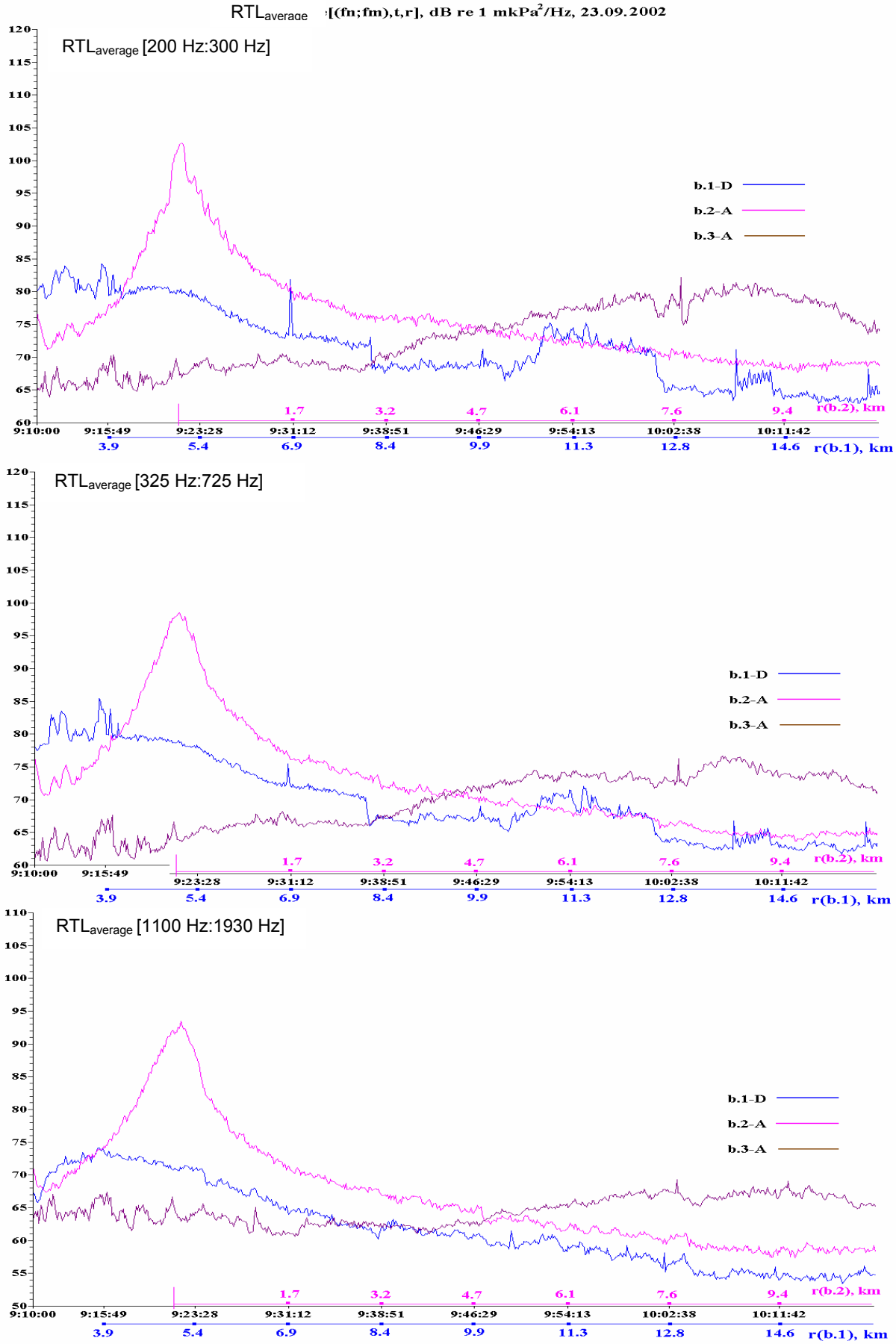

Figure 4.7 - Plots of *RTL*$_{average}$ calculated with Equation (10) using noise generated by the *Trias* and recorded on sonobuoys b.1, b.2 (digital), and b.3 (analog).

Equation (10) is the optimum algorithm to use to estimate the relationship between relative transmission loss frequency and range [RTL(f,r)] for noise produced by a moving source (i.e. analyze $RTL_{average}$ [Δf,f,r]). Combined analysis of the experimental data displayed on Figures 4.4, 4.7 and 4.8 allow RTL(f,r) to be estimated for the area.

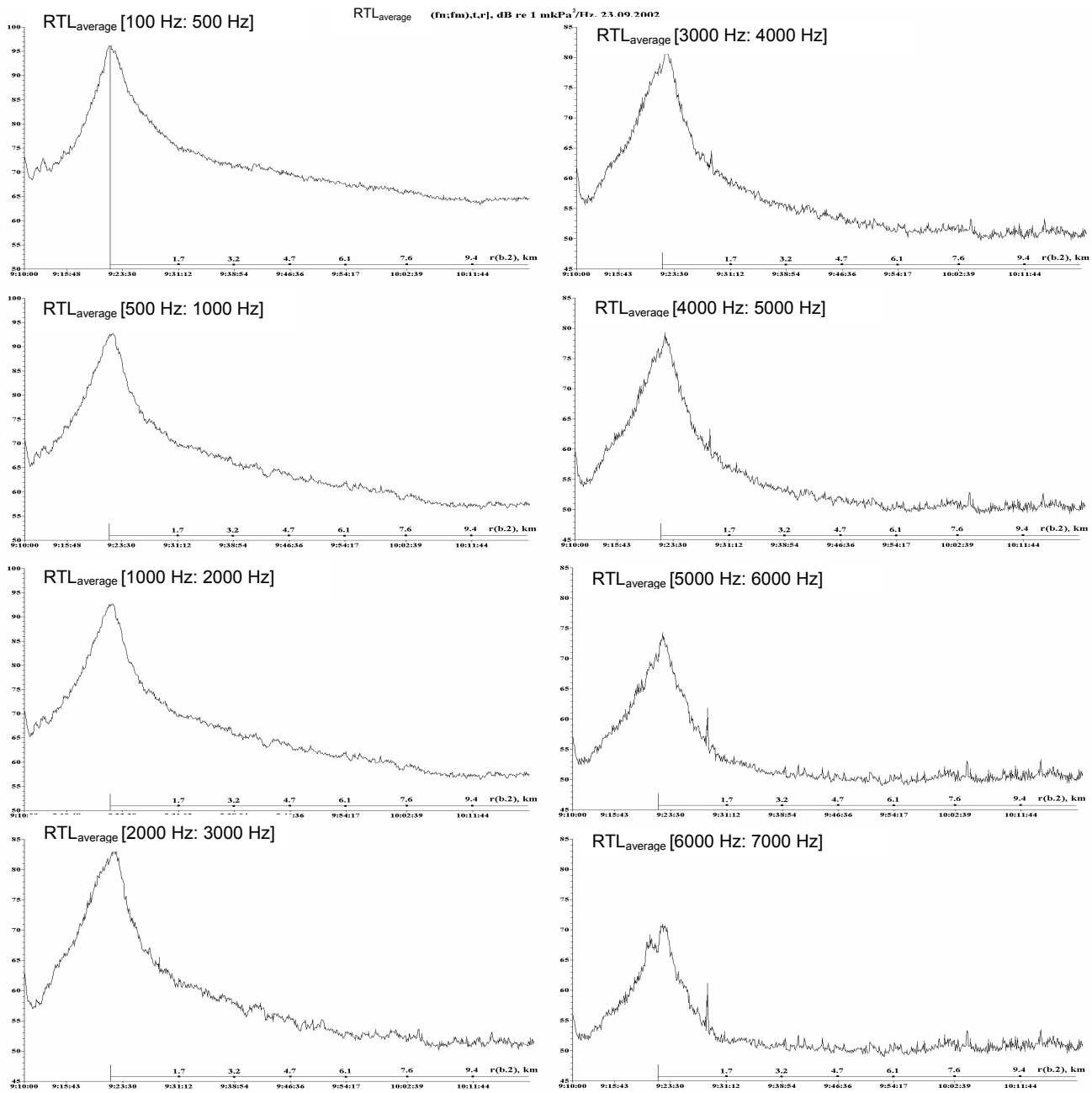

Figure 4.8 - Plots of $RTL_{average}$ calculated with Equation (10) using noise generated by the *Trias* and recorded on sonobuoy b.2 (digital).

The preceding section showed the results of a TL study in the Chayvo area using signals generated by HF and LF transducers. The propagation of anthropogenic noise generated by equipment on or near the barge quay was also investigated. As the noise source was unknown an analysis of the relative transmission loss (RTL) between b.1 and b.2 was conducted. RTL was defined as the difference between the levels of signals synchronously recorded at both points. Additionally, the results from model studies of sound propagation and TL from b.1 to b.2 using the model shown in Figure 4.9 were also analyzed.

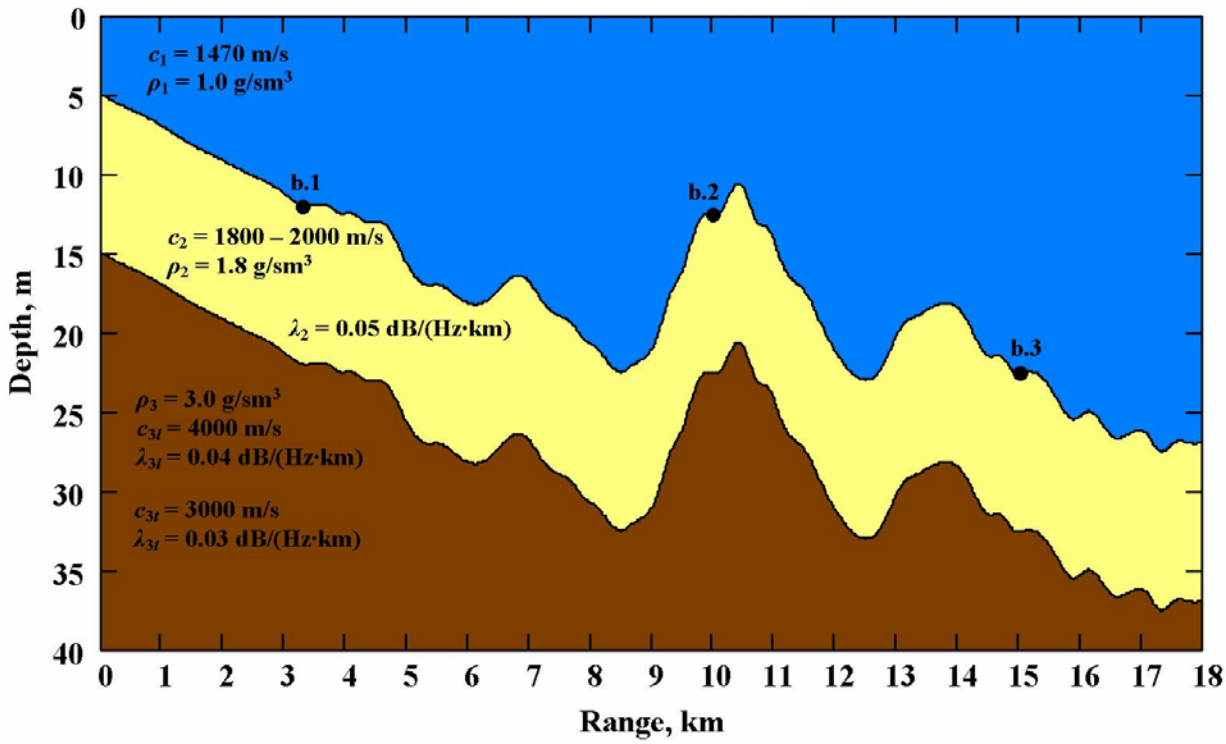

Figure 4.9 - Chayvo acoustic model showing the model parameters.

The program MOATL was used for the acoustic modeling[36]. The goal of the modeling was to find the bottom profile parameters that best matched the experimental results.

The model waveguide consists of three layers, a homogeneous water layer, a 10 m thick sediment layer and a bedrock layer, the model parameters are given on Figure 4.9. The bathymetric profile was built using echosounder data recorded in the field. The source was located on the water bottom at the start of the profile (Range=0).

[36] The program uses an adiabatic mode theory approximation for calculating TL in a waveguide.

Figure 4.10 shows the variation in relative TL (RTL) with frequency for both the experimental and model data. Experimental data for different dates are shown in different colors, the model results are shown by a blue line with open circles showing the frequencies for which an RTL estimate was computed.

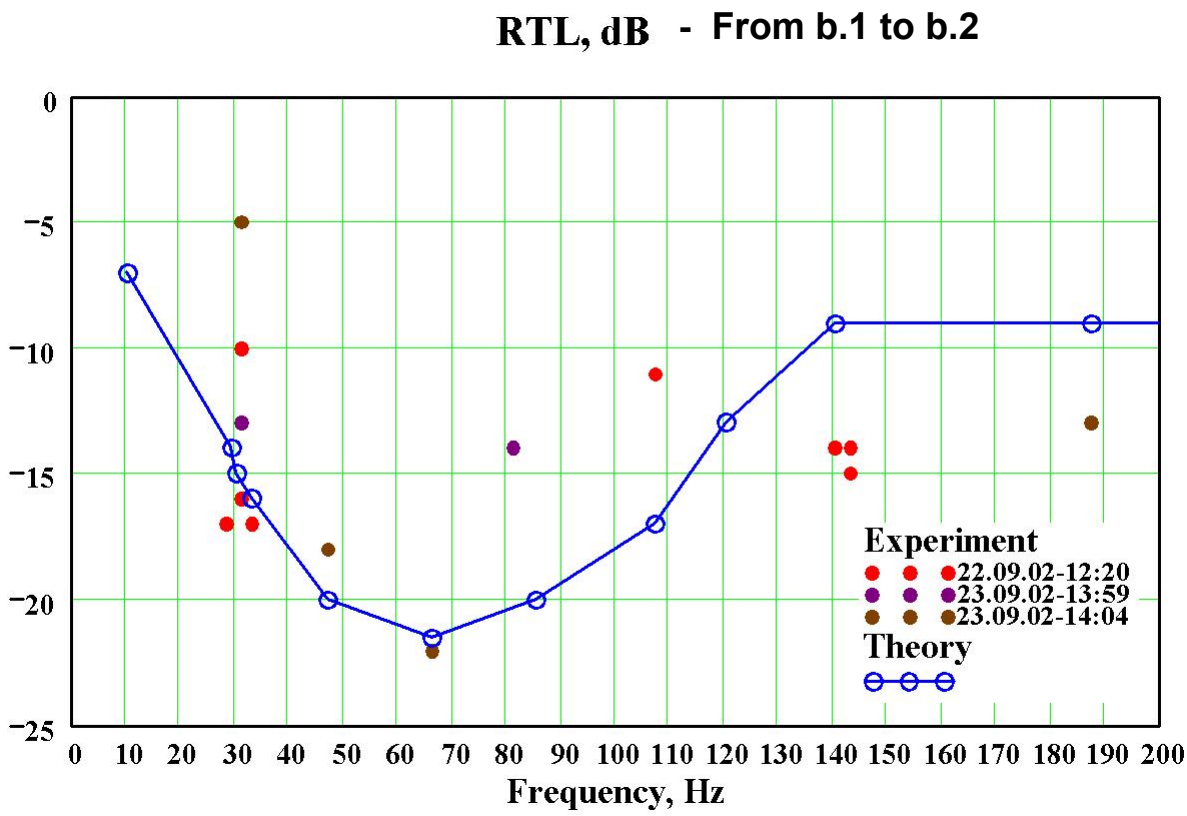

Figure 4.10 - Experimental and Model RTL data from the Chayvo acoustic experiment.

Figure 4.11 shows an analysis of noise generated by the vessel *Trias* as it passed location b.2 on the morning of 23 September. Figure 4.7 gives the temporal (and spatial) dependence of noise generated by the *Trias* and recorded at location b.2, computed using Equation (10). Figure 4.11[37] gives RTL-range graphs, estimated from the decreasing noise level as the *Trias* moved away from its maximum intensity point. RTL values for different frequency bands are in different colors, the range scale is logarithmic.

[37] Data plotted in Figure 4.11 is from Figure 4.7.

Regression was used to estimate the logarithmic rate of decrease in intensity with range r. The regression used the equation:

$$RTL(r)=a*\log(r)+b. \qquad (16)$$

The regression results use the same colors as the experimental data and show very weak dependence on the level of acoustic noise. The regression shows that in the band from 200-300 Hz the intensity decreases at 18 dB/decade, from 325-725 Hz at 16 dB/decade and from 1100-1930 Hz at 19 dB/decade.

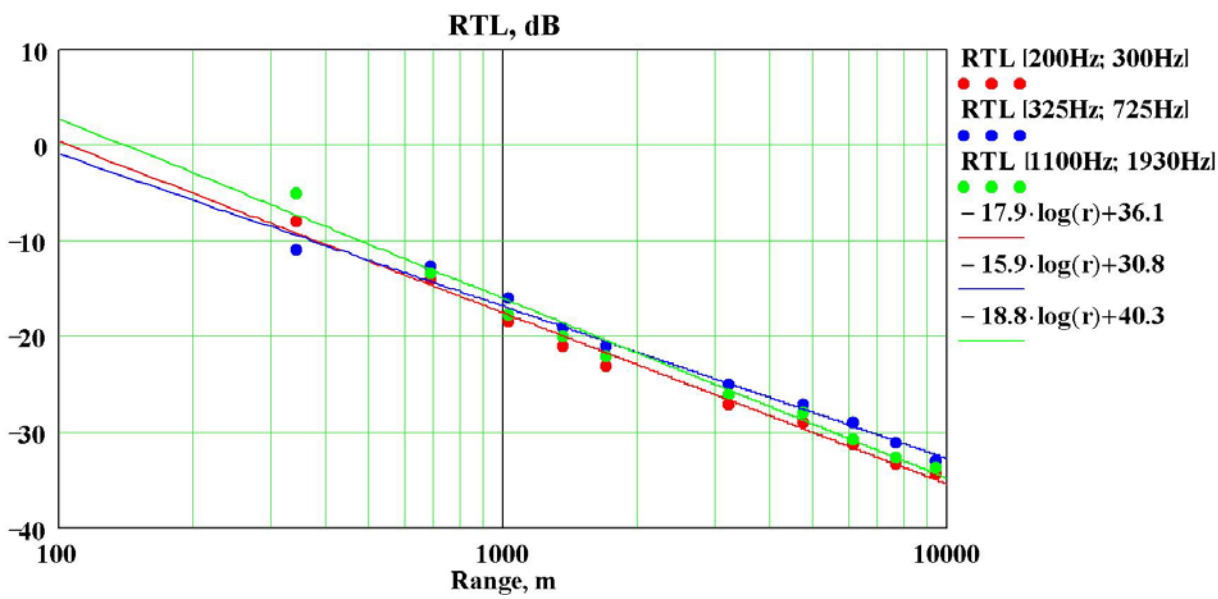

Figure 4.11 - Plot of RTL vs Range for the *Trias* experiment of 23 September, the data were plotted on Figure 4.7.

5 Conclusions

1. The new digital sonobuoys performed well. They recorded data for frequencies from 1-2600 Hz and when paired with an analog sonobuoy were used to record acoustic data in the band from 1 Hz -10 kHz. Synchronous measurements of broadband noise both at the source and receivers allow an accurate estimation of the TL between the source and the sonobuoy.
2. Three TL experiments were conducted from the area near the Molikpaq platform to near the mouth of Piltun Bay, the frequency dependent TL estimated from these experiments is given in Tables 3.1, 3.2 and 3.3.

   For a distance of 19.2 km (Table 3.2), the estimated TL was:

Frequency (Hz)	1000	2000	3000	4000	5000	6000	7000	8000	9000
Estimated TL (dB)	~-76	~-90	~-83	~-93	~-96	~-95	~-95	~-108	~-111

   Regression on all the Molikpaq-Piltun TL data assumed that the estimated TL could be approximated by the set of equations below and regressed the data to determine the coefficients:

$$TL = \begin{cases} -20\log(r) & ; r \le r_1 \\ -15\log(r) - 5\log(r_1) - \beta_1(r - r_1) & ; r_1 < r \le r^* \\ -10\log(r) - 5\log(r_1) - 5\log(r^*) - \beta_1(r^* - r_1) - \beta(r - r^*) & ; r^* < r \end{cases}$$

   The values of β_1, β, r^*, and r_1 as well as the regression errors are given in Table 3.4 for frequencies between 1-9 kHz. The regression shows an increase in the attenuation coefficients with increasing frequency.
3. A significant component of the TL at frequencies below 40 Hz is bottom absorption, the TL at low frequencies can be generally approximated using the equation:

$$TL = -10\log(r) - 10\log(r_1) - \beta(r - r_1)$$

Where:

$$r_1 \approx \frac{H^2}{2\lambda}$$

H is the waveguide depth

λ is the wavelength

β is the absorption coefficient for compressional waves, it has been experimentally estimated using both impulsive and CW data as 0.12 dB/km/Hz.

4. Due to operational restrictions near the Chayvo barge quay it was not possible to conduct a TL experiment from close inshore, the TL experiments conducted both up slope and down slope gave variations in TL with range that were similar to those obtained on the Molikpaq-Piltun transect.
5. Both experimental results from TL experiments with moving vessels in the Chayvo area and theoretical results from models indicate that the TL reaches a maximum in the frequency band from 30 to 70 Hz. For example in the Chayvo area the relative TL (RTL) at 65 Hz is approximately 10 dB greater than the RTL at 30 Hz and 109 Hz.
6. As the *Trias* departed the area the data was used to estimate relative TL. This data can be used to make an estimate of the RTL in different frequency bands. For frequencies higher than 1 kHz there is a near field zone ($r < r_1 \approx 0.2$-1.8 km) where the sound level decreases proportionally to -20log(r). Beyond this zone, the sound level decreases proportionally to -19log(r) ($r > r_1$), for frequencies above 1 kHz and proportionally to -18*log(r)* for frequencies between 200-300 Hz.

6 Future plans

The development of digital sonobuoys by POI has significantly increased the dynamic range and bandwidth of the acoustic data recorded in 2002. A digital sonobuoy with a 16-bit ADC (96 dB) and encoding, can transmit signals between 0-2500 Hz. If the 12-bit ADC (72 dB) is used, then the frequency range is 0-4000 Hz. One of the main advantages of digital encoding is the elimination of system noise and electrical induction, which are particularly significant at low frequencies and preclude accurate measurements of infrasounds by analog sonobuoys. The combination of digital and analog sonobuoys will allow accurate acoustic measurements from 1 to 10,000 Hz (digital 1-2500 Hz, analog 200-10,000 Hz).

However, the dynamic range and radio-reception limits of the analog and digital sonobuoys have demonstrated the need to develop new autonomous digital recording equipment. In 2003, a new Autonomous Underwater Acoustic Recorder (AUAR) will be developed with the dynamic range of the digital sonobuoy electronics, but without the bandwidth limitations of sonobuoy radio transmission. These recorders will be self-contained, having the power and storage capacity to record continuously for approximately 14 days.

The digital AUAR will have a 16-bit ADC (96 dB), a 60 GB hard drive, and hydrophones calibrated from 1 Hz to 10 kHz. The AUAR's will be dual channel, one channel sampling at 20 kHz and one 30 kHz with a selectable low cut filter to maximize the dynamic range of the higher frequency channel. This will allow accurate acoustic measurements to be made from 1 to 15,000 Hz. The AUAR can record both channels together, or, only the 20 kHz channel. The recording protocol will be a balance between record time, disk and power.

The acoustic studies conducted in the Molikpaq and Chayvo areas in 2002 confirmed that synchronous signals recorded by multiple sonobuoys could be used for effective TL experiments. Any acoustic measurements undertaken in a high current regime such as the NE Sakhalin shelf can be effected by flow noise due to the interaction of the water flow with the stationary hydrophone. This can bias low frequency (<25 Hz) acoustic measurements and make studies of low frequency transmission loss difficult. POI is investigating recording and analysis methods to reduce the effect of this noise on TL measurements.

7 Acknowledgements

The authors would like to thank the V.I. Il`icev Pacific Oceanological Institute, FEB Academy of Sciences of Russia (POI), for permission to conduct this work.

The authors would also like to acknowledge the following personnel from POI, who while they did not contribute to the report, contributed significantly to the success of the program in the field. Scientists: Sc. S.V. Borisov (Борисов С.В.), A.V. Gritsenko (Гриценко А.В.), A.V. Hodzevich (Ходзевич А.В.), R.A. Korotchenko (Коротченко Р.А.); engineers: E.A. Maslennikov (Масленников Е.А.), V.V. Lihachev (Лихачев В.В.), D.G. Kovzel` (Ковзель Д. Г.).

The authors also wish to thank the crew of the *Irbis* for their hospitality and assistance while conducting acoustic measurements in the vicinity of Odoptu, Molikpaq and Chayvo.

Finally the authors would like to thank Dr. Sc. G.I. Dolgih (Долгих Г. И.)(POI), Dr. Richard T. Houck, Dr. H. Rodger Melton (ExxonMobil Upstream Research Co.) and Dr. Charles I. Malme (Engineering and Scientific Services) for reviewing this report.

Our special thanks go to the investment companies, their employees and consultants, without whom the present work could not have been conducted. These include:
LGL Limited. - Dr. S.B. Yazvenko and Dr. S.R. Johnson
Exxon Neftegas Limited. - M. Esengalieva, M.R. Jenkerson, C.R. Martin and H.R. Melton
Sakhalin Energy Investment Company Limited. - A. Onder and S. Balytsok

8 Authors

From the V.I. Il`icev Pacific Oceanological Institute, Far East Branch, Academy of Sciences of Russia:
Sc. M.V. Kruglov (Круглов М.В.)
Dr. Sc. A.N. Rutenko (Рутенко А.Н.)

9 Bibliography

1. Borisov S.V., Gritsenko A.V., Jenkerson M.R., Rutenko A.N., and Hodzevich A.V. (2002) Evaluating and Monitoring Acoustic Transmission from the Odoptu 3D seismic Survey 5 August - 9 September, 2001; Sakhalin, Russian Federation. Pacific Oceanological Institute (FEB RAS) report for Exxon Neftegas Ltd.
2. Borisov S.V., Gritsenko A.V., Rutenko A.N., and Hodzevich A.V. (2003a) Results of Acoustic Studies Within and Adjacent to the Piltun-Astokh License Area 1 to 6 August, 2001 and 17 to 24 September, 2001; Sakhalin, Russian Federation. Pacific Oceanological Institute (FEB RAS) report for Exxon Neftegas Ltd. & Sakhalin Energy Investment Company.
3. Borisov S.V., Gritsenko A.V., Kruglov M.V., Korotchenko R.A., and Rutenko A.N. (2003b) Results of Acoustic Studies between Molikpaq and Piltun and Near Chayvo Bay 12 September to 23 September, 2002; Sakhalin, Russian Federation. Pacific Oceanological Institute (FEB RAS) report for Exxon Neftegas Ltd. & Sakhalin Energy Investment Company.
4. Brekhovskikh, L.M. (1974). Waves in layered environment. Nauka Publisher, Moscow. 343 p.
5. Ashley C.E., Siegman W.L., Jacobson M.J. (1987) Random bottom structured and topographical effects on sound transmission in shallow channel. Ibid. 1987. vol. 81 (3), pp. 650-659.
6. Katsnelson B.G., Petnikov V.G. (1997). The acoustics of a shallow sea. Nauka Publisher, Moscow. 188 p.
7. Hampton R.L. (1974). The acoustics of marine sediments. Ed: R.L. Hampton. Mir Publisher, Moscow. 498 p.
8. Cooperman U., Jensen F. (1984). The acoustics of Ocean bottom. Eds. Cooperman U., Jensen F. Mir Publisher, Moscow. 454 p.
9. Biot M. (1956) Theory of propagation of elastic waves in a fluid-saturated porous solid. Ibid. Vol. 28 (1), pp. 168-191.
10. Jensen F.B., Cooperman U.A. (1985). Deterministic models of noise propagation. In: Underwater acoustics and signal analysis. Ed. L. Bjorn. Mir Publisher, Moscow. p. 125-134.
11. Bespalov L.A., Derzhavin A.I., Kudryavtsev O.V., Semenov A.G. (1998). Estimation of the influence of bottom layers on the seismic field of a low-frequency source on the

Oceanic shelf. In: The acoustics of the Ocean. Proc. VII workshop of Acad. L.M. Brekhovskikh.

12. McDoniel S.T. (1982) Mode coupling due to interaction with the seabed. J. Acoust. Soc. Amer. Vol. 72. №6, pp. 916-923.
13. McDoniel S.T., McCammon D.F. (1987) Mode coupling and the environmental sensitivity of shallow-water propagation loss predictions. J. Acoust. Soc. Amer. Vol. 82, pp. 217-223.
14. Zhou J.X., Zhang X.Z., Rogers P.H. (1991) Resonant interaction of sound wave with internal solitons in the coastal zone . J. Acoust. Soc. Amer. Vol. 90. № 4, pp. 2042-2054.
15. Borodin V.V., Zhuravlev V.A., Kobozev I.K. Kravtsov Yu.A. (1992). Averaged parameters of acoustic fields in oceanic channels. Akusticheskij Zhurnal, 38: 601-608.
16. Brekhovskikh L.M. (1965). Averaged field in underwater acoustic channel. Akusticheskij Zhurnal, 11: 148-159.
17. Katsnelson B.G., Petnikov V.G. (1997). The acoustics of a shallow sea. Nauka Publisher, Moscow. 188 p.
18. Kravtsov Yu.A., Orlov Yu.I. (1980). Geometric optics of anisotropic environment.
19. Borisov S.V., Kabanov N.F., Rutenko A.N. (1996) Experimental study of sound field fluctuations on fixed paths. Acoustical Physics. vol. 42 № 3, pp. 301-311 / Translated from Akusticheskii Zhurnal. 1996. vol. 42. № 3, pp. 347-358
20. Brekhovskikh L.M. M. GEOS. p. 104-108.
21. Sobolevsky E.I., et.al. (1999) Report for Sakhalin Energy Investment Company.
22. Sobolevsky E.I., et.al. (2000) Report for Sakhalin Energy Investment Company.
23. Richardson W.J., Greene C.R., Malme C.I. and Thomson D.H. (1995). Marine mammals and noise. Academic Press Limited. 576 p.
24. Bondar` L.F., Gritsenko A.V., Zakharov V.A., Kovzel` D.G. and Rutenko A.N. Digital radiotelemetry system for the collection and results of its application in studies of sea reverberation characteristics. Acoust. Phys., 1993, vol.39, no.2, pp.118-122.

Appendix A - TL for propagation parallel and perpendicular to the coast[38]

To evaluate the attenuation of acoustic energy generated by air guns on the *Nordic Explorer,* a series of acoustic experiments were conducted prior to the start of the seismic survey. The purpose of these studies was to measure the received level (RL) of the acoustic signal at the 10 m and 20 m contours. In order to estimate the variation in RL throughout the survey area, experiments were conducted in both the northern and southern part of the 3D survey area. For these studies the *Nordic Explorer* fired its air guns (production array) while sailing along lines perpendicular or parallel (the shooting direction of the survey) to the shoreline. Receivers were stationed at depths of 20 m and 10 m or 6 m. The layout of the southern experiment is shown at the top of Figure B.1.

Figure B.1 also shows plots of the rms and peak values for acoustic data recorded by sonobuoys at locations T.1.3 and T.2 while the *Nordic Explorer* was sailing from east to west. Figure B.1 also shows transmission loss (TL) formulas for calculating range (R) dependent attenuation. For TL estimates of 20logR and 40logR the signal level at a distance of 1 km from the source was 160 dB and 184 dB re 1 μPa respectively.

Figures B.2 and B.3 show the TL for acoustic profiles parallel and perpendicular to the shore. Figure B.2a shows the rms values for acoustic pulses received at locations T.4, T.4.2 and T.5 for data acquired while the *Nordic Explorer* was sailing along a line parallel to the shoreline[39]. Figure B.2b shows data acquired while the *Nordic Explorer* was sailing along a line perpendicular to the shoreline[40]. This data describes the attenuation of seismic impulses in the northern part of 3D area.

Figure B.3 shows rms values for seismic impulses recorded at locations T.7 and T.11, this data was acquired while the *Nordic Explorer* sailed the closest source line parallel to the shoreline. The purpose of the study was to determine the TL for an acoustic profile parallel to bathymetry; this would be compared with the TL for a profile perpendicular to bathymetry.

---

[38] This section is excerpted from Borisov et al., 2002.
[39] Line acquired 13 August 2001, from 18:10 to 19:20.
[40] Line acquired 13 August 2001, from 22:03 to 22:25.

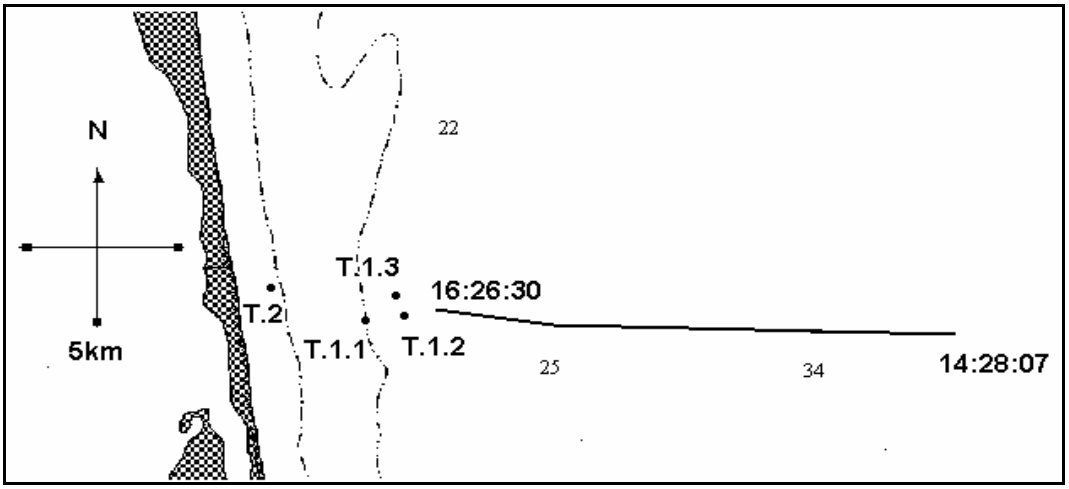

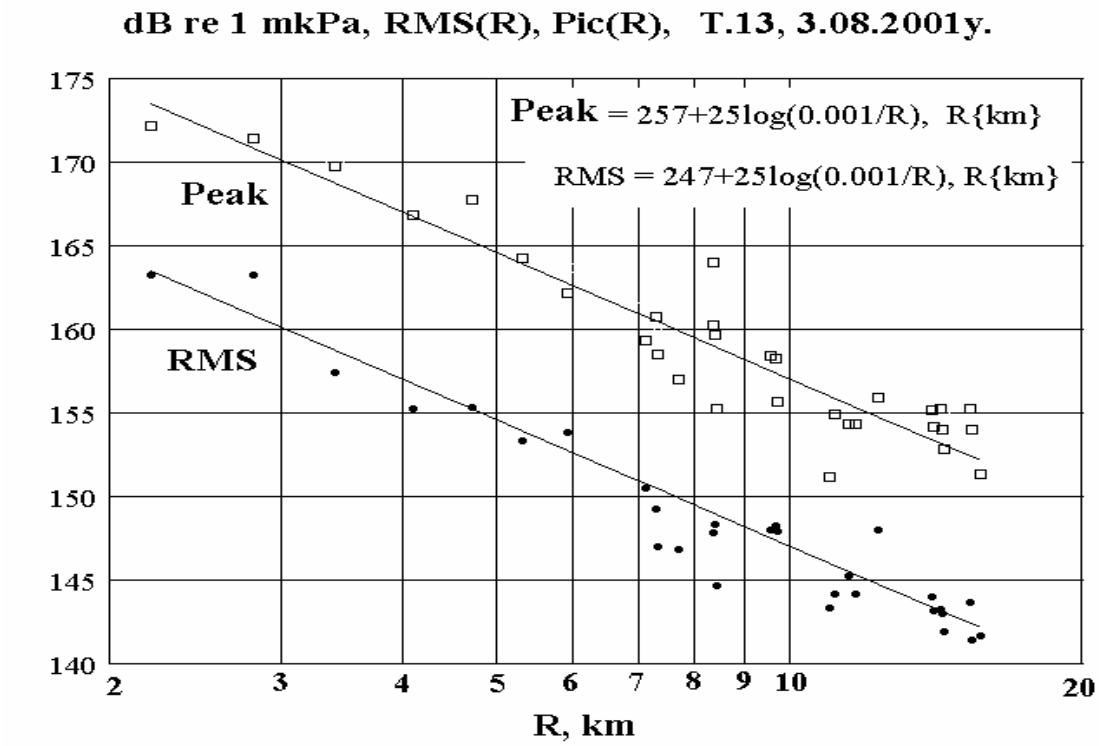

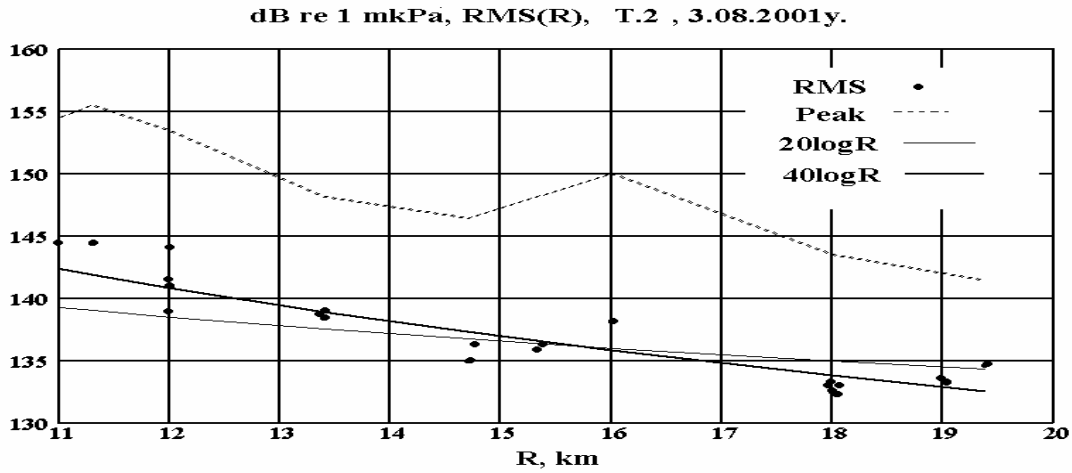

Figure B.1 - Layout of the southern TL study, peak and rms data from buoy T.1.3 and peak and rms data from buoy T.2.

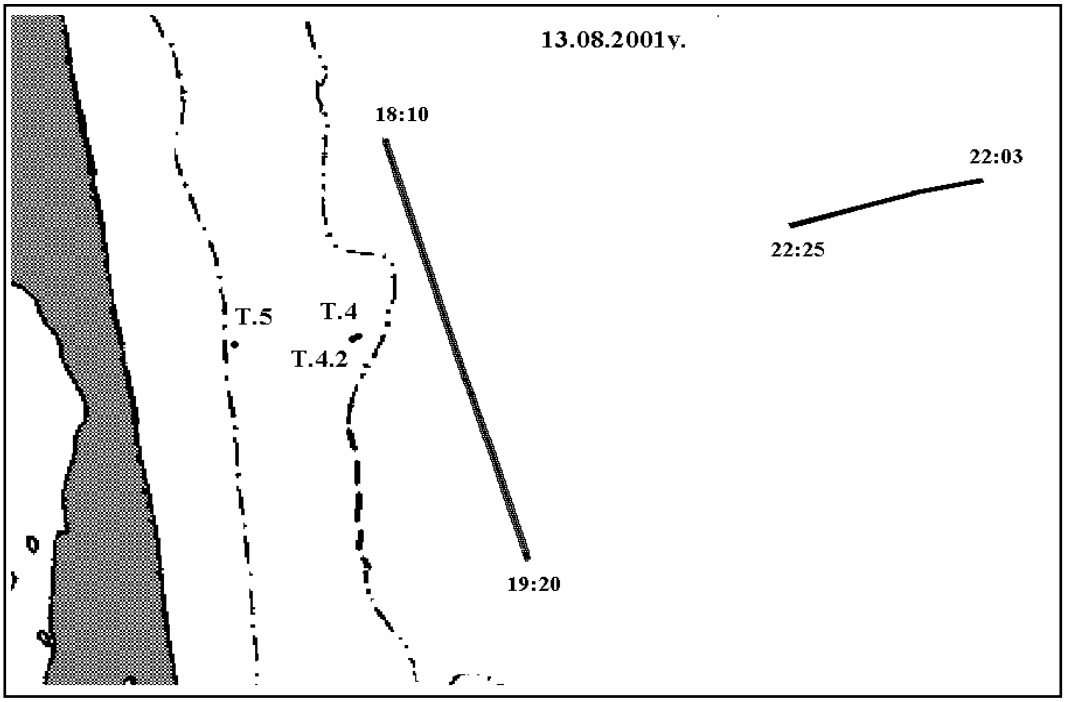

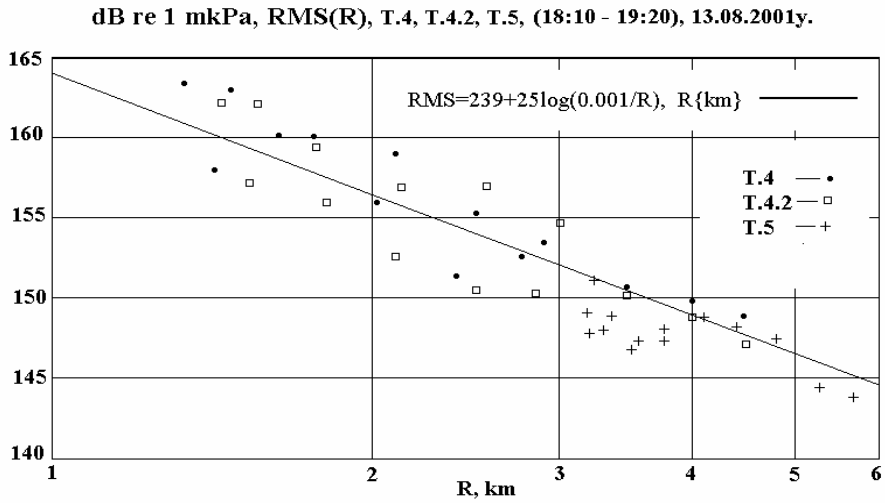

a.

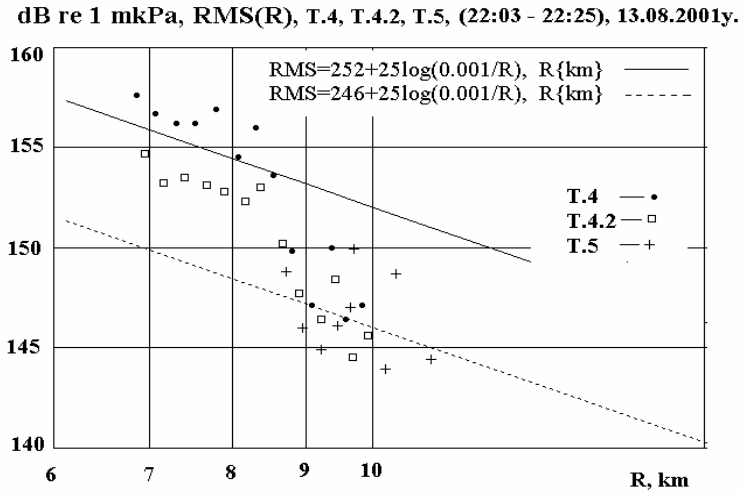

b.

Figure B.2 - Layout of the northern TL study, peak and rms data from buoys T.4, T.4.2 and T.5 for profiles perpendicular (a) and Parallel (b) to the coast.

Figures B.1 to B.3 show that the attenuation of acoustic pulses in the 3D area does not depend on attitude to bathymetry. The TL to the 20 m contour (from deeper water) can be estimated using TL=-25log(R), where R is the distance between source and receiver (m).

The results from these TL experiments can be used in modeling acoustic propagation for a profile perpendicular to the shoreline in a location with bathymetry and hydrology similar to the Odoptu area (like Figure B.1).

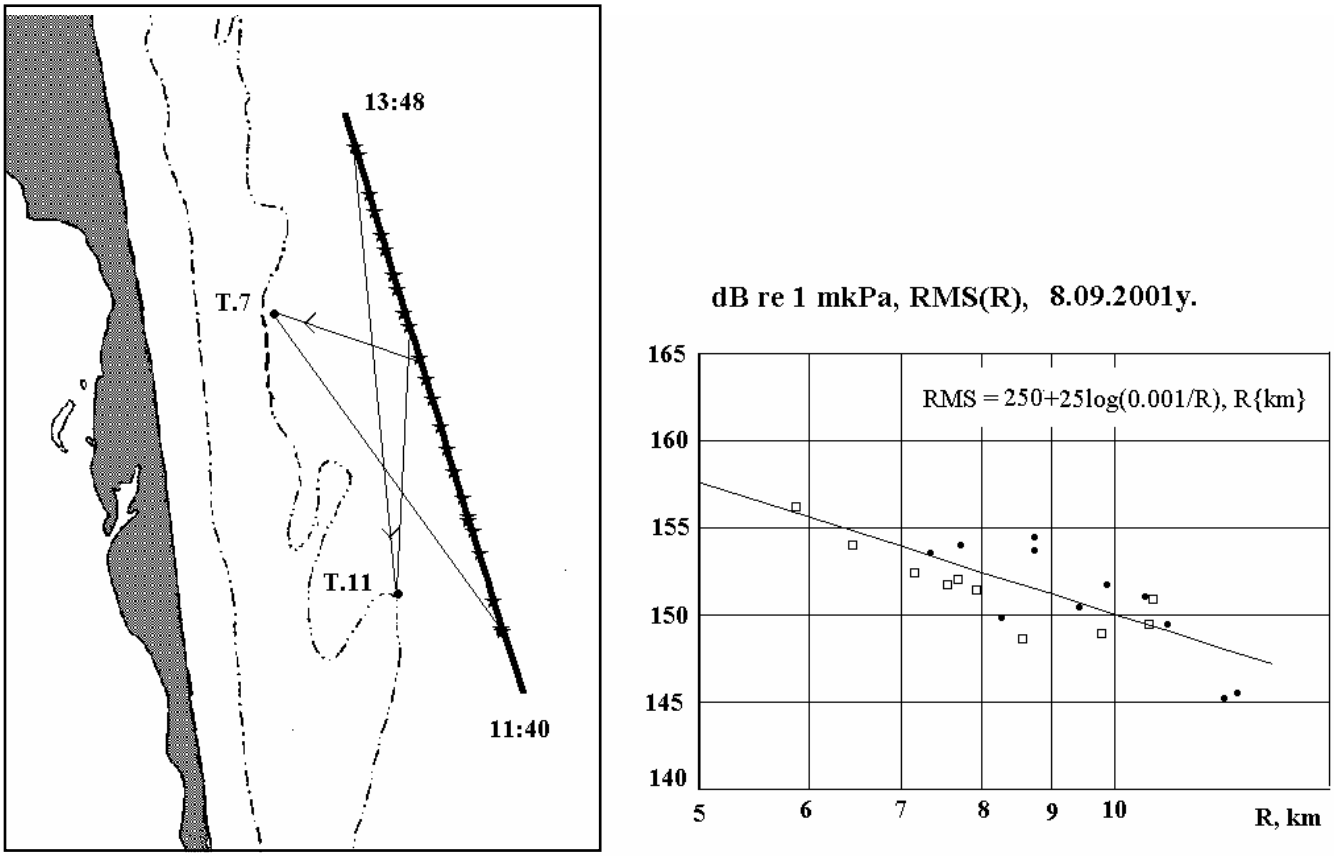

Figure B.3 - TL study for propagation parallel to bathymetry, rms data from buoys T.7 and T.11 for a profile parallel to the coast.

Appendix B - Description of data used for the TL studies

Tables B.1 and B.2 give the coordinates of the sonobuoys used in the study and plotted in Figures 3.1 and 4.1, the start and completion of acoustic recording with each sonobuoy as well as the deployment depth of their hydrophones.

Table B.1 - Operational dates and locations of monitoring Sonobuoys [Molikpaq-Piltun transect].

№	Date		Sonobuoy			Latitude	Longitude	Depth
	Begin	Finish	#	Type	F(MHz)			(m)
1	19.09.02	20.09.02	a.0	ARB	188.030	52°59'43"N	143°19'14"E	10.5
2	12.09.02 12.09.02 15.09.02	19.09.02 14.09.02 22.09.02	a.1 a.1 a.1	ARB D12 D12	188.030 166.720 166.720	52°52'00"N	143°20'50"E	10
3	12.09.02 15.09.02	19.09.02 19.09.02	a.2 a.2	ARB D16	177.300 166.775	52°49'44.1"N	143°24'06.3"E	21
4	13.09.02 13.09.02	19.09.02 19.09.02	a.4 a.4	ARB D16	176.650 166.125	52°44'59.9"N	143°31'01"E	27
5	13.09.02 13.09.02	19.09.02 15.09.02	a.5 a.5	ARB D16	172.400 166.775	52°43'28"N	143°33'06.4"E	32

Table B.2 - Operational dates and locations of monitoring Sonobuoys [Chayvo transect].

№	Date		Sonobuoy			Latitude	Longitude	Depth
	Begin	Finish	#	Type	F(MHz)			(m)
1	21.09.02 21.09.02	23.09.02 23.09.02	b.1 b.1	ARB D16	172.400 166.775	52°27'00"N	143°19'30"E	12.5
2	21.09.02 21.09.02	23.09.02 23.09.02	b.2 b.2	ARB D16	176.650 166.125	52°47'40"N	143°22'30"E	12.5
3	21.09.02	23.09.02	b.3	ARB	177.300	52°21'00"N	143°26'30"E	22.5